Development/Plasticity/Repair

Enhanced Recruitment of Endosomal Na^+/H^+ Exchanger NHE6 into Dendritic Spines of Hippocampal Pyramidal Neurons during NMDA Receptor-Dependent Long-Term Potentiation

Emily C. Deane,[1]* Alina E. Ilie,[2]* Saman Sizdahkhani,[1] Micaela Das Gupta,[1] John Orlowski,[2] and R. Anne McKinney[1,3]

[1]Department of Neurology and Neurosurgery, [2]Department of Physiology, and [3]Department of Pharmacology and Therapeutics, McGill University, Montreal, Canada

Postsynaptic endosomal trafficking has emerged as a principal regulatory mechanism of structural and functional plasticity of glutamatergic synapses. Recycling endosomes perform activity-dependent transport of AMPA receptors (AMPARs) and lipids to the postsynaptic membrane, activities that are known to contribute to long-term synaptic potentiation and hypothesized to subserve learning and memory processes in the brain. Recently, genetic defects in a widely expressed vesicular pH-regulating transporter, the Na^+/H^+ exchanger NHE6 isoform, have been implicated in neurodevelopmental disorders including severe X-linked mental retardation and autism. However, little information is available regarding the cellular properties of this transporter in the CNS. Here, we show by quantitative light microscopy that the protein abundance of NHE6 is developmentally regulated in area CA1 of the mouse hippocampus. Within pyramidal neurons, NHE6 was found to localize to discrete puncta throughout the soma and neurites, with noticeable accumulation at dendritic spines and presynaptic terminals. Dual immunolabeling of dendritic spines revealed that NHE6 partially colocalizes with typical markers of early and recycling endosomes as well as with the AMPAR subunit GluA1. Significantly, NHE6-containing vesicles exhibited enhanced translocation to dendritic spine heads during NMDA receptor (NMDAR)-dependent long-term potentiation. These data suggest that NHE6 may play a unique, previously unrecognized, role at glutamatergic synapses that are important for learning and memory.

Introduction

During development and learning-related plasticity, dynamic alterations in synapse composition and structure are responsible for establishing proper connectivity in the brain. At excitatory synapses in the CNS, endosomal trafficking has emerged as a principal regulatory mechanism of morphological and functional plasticity (Ehlers, 2000; Park et al., 2006; Petrini et al., 2009). In particular, activity-dependent endosomal recycling of glutamatergic AMPARs and lipid membranes are known to modulate synaptic strength and morphology of dendritic spines, the postsynaptic component of most excitatory synapses in the cortex and hippocampus (Yuste and Bonhoeffer, 2001; Kennedy and Ehlers, 2006). Experimental manipulations that disrupt the trafficking of recycling endosomes have been shown to block long-term potentiation (LTP), a well established model of learning and memory, and can even result in spine loss (Park et al., 2004, 2006). Hence, there has been intense interest in unraveling the molecular mechanisms that underlie the trafficking of endosomes at dendritic spines and how they impact synaptogenesis and plasticity.

To this end, studies have begun to identify components of the molecular machinery that govern the trafficking of these vesicles at the postsynaptic compartment. These include certain SNAREs (Kennedy et al., 2010; Lau et al., 2010; Suh et al., 2010), synaptotagmins (Dean et al., 2012), Rab-GTPases (Brown et al., 2005; Park et al., 2006), components of the exocyst complex (Gerges et al., 2006), and actin-based molecular motors (Wang et al., 2008). Acidification of vesicles is also an important determinant of their biogenesis and function (Weisz, 2003), yet the mechanisms controlling pH homeostasis of postsynaptic endosomes are not well understood. The importance of intravesicular acidification is highlighted by recent reports of genetic defects in certain alkali

Received May 29, 2012; revised Oct. 2, 2012; accepted Nov. 7, 2012.

Author contributions: J.O. and R.A.M. designed research; E.C.D., A.E.I., S.S., and M.D.G. performed research; A.E.I. and J.O. contributed unpublished reagents/analytic tools; E.C.D. and A.E.I. analyzed data; E.C.D., A.E.I., J.O., and R.A.M. wrote the paper.

This work was supported by Canadian Institutes of Health Research funding held by R.A.M. (MOP-86724) and J.O. (MOP-11221 and MOP-111191). E.C.D. held a McGill Provost's Graduate Fellowship and received funding from the ARSACS Foundation. M.D.G. received a Natural Sciences and Engineering Research Council of Canada Studentship. R.A.M. held a Le Fonds de la Recherche en Santé de Québec Senior Salary Bursary during the period of this work. We thank François Charron, Philip K.-Y. Chang, David Verbich, Haider Altimini, and Tushare Jinadasa for their technical assistance. We also thank Dr. David Stellwagen for generously providing us with DNA constructs and Dr. Keith Murai for assistance with experimental design and for critical reading of this manuscript. We also acknowledge the technical assistance provided by the McGill Life Sciences Imaging Facility, the Electron Microscopy Facility of the Department of Pharmacology and Therapeutics (McGill University), and Genome Quebec.

*E.C.D. and A.E.I. contributed equally to this work.

The authors declare no competing financial interests.

Correspondence should be addressed to either of the following: Dr. R. Anne McKinney, Department of Pharmacology and Therapeutics, Bellini Life Science Complex, Room 167, 3649 Promenade Sir William Osler, McGill University, Montreal, Quebec, H3G 0B1, Canada, E-mail: anne.mckinney@mcgill.ca; or Dr. John Orlowski, Department of Physiology, Bellini Life Science Complex, Room 166, 3649 Promenade Sir William Osler, McGill University, Montreal, Quebec, H3G 0B1, Canada. E-mail: john.orlowski@mcgill.ca.

DOI:10.1523/JNEUROSCI.2583-12.2013

 0270-6474/13/330595-16$15.00/0

cation/H^+ exchangers (*SLC9A* gene family, commonly called Na^+/H^+ exchangers; NHEs), NHE6 and NHE9, that are widely expressed and targeted to recycling endosomes, but curiously cause severe forms of X-linked mental retardation (Gilfillan et al., 2008; Garbern et al., 2010) and autistic behavior (Morrow et al., 2008). In non-neuronal cells, overexpression and knockdown of NHE6 were found to regulate clathrin-mediated endocytosis of selected cargo (i.e., transferrin receptors, Tf-Rs) and maintenance of cell polarity in a manner that was dependent on its ability to modulate intravesicular pH (Ohgaki et al., 2010, Xinhan et al., 2011). However, the distribution and physiological roles of these transporters in the CNS remain largely uncharacterized.

In this report, we generated an NHE6-specific antibody to investigate its expression in mouse hippocampus, a region important for learning and memory. In tissue sections and organotypic slices, the abundance of NHE6 increased significantly during postnatal development of area CA1. In CA1 pyramidal neurons, NHE6 was detected throughout the soma and dendrites in puncta that were enriched at dendritic spines, but also at excitatory presynaptic terminals. Dual immunolabeling analyses showed that NHE6 partially colocalized with known markers of early and recycling endosomes, as well as with the AMPAR subunit GluA1. Significantly, following NMDAR-dependent LTP, NHE6-containing vesicles were recruited to dendritic spines, alterations that may have important implications for learning and memory.

Materials and Methods

Antibodies and reagents. Chemicals and reagents used for AP-1 and SH-SY5Y cell culture were obtained from either BioShop Canada or Fisher Scientific, with the exception of α-Minimum essential medium (α-MEM), fetal bovine serum (FBS), penicillin/streptomycin, and trypsin-EDTA, which were purchased from Invitrogen. All products used for neuronal organotypic slice and primary cell culture were purchased from Gibco/Invitrogen unless otherwise indicated. Protein localization studies using immunofluorescence and immunoblotting were performed using the following commercial antibodies: mouse monoclonal anti-hemagglutinin (HA) antibody (Covance), rabbit polyclonal anti-HA (Abcam), anti-β-tubulin antibody (Sigma-Aldrich), anti-transferrin receptor antibody (Invitrogen), mouse monoclonal anti-syntaxin-12/13 (Stx-13; Synaptic Systems), mouse monoclonal early endosomal antigen 1 (EEA1; Sigma), and mouse monoclonal anti-GluA1 (GluA1/GluR1; Synaptic Systems). The rabbit polyclonal anti-TOM70 antibody was a kind gift from Dr. Jason Young (McGill University, Montreal). Alexa Fluor 568-conjugated transferrin (AF-Tfn) was purchased from Invitrogen. Secondary antibodies used in this study include horseradish peroxidase (HRP)-conjugated secondary IgG antibodies (Jackson ImmunoResearch), Alexa Fluor 594 goat anti-rabbit IgG (Invitrogen), Alexa Fluor 647 goat anti-rabbit IgG (Invitrogen), Cy5 goat anti-mouse IgG (Millipore), and Dylight649 goat anti-rabbit IgG (Jackson ImmunoResearch). The green fluorescent protein (GFP)-tagged superecliptic pHluorin attached to AMPAR subunit GluA1 (SEP-GluA1) was a kind gift from Dr. David Stellwagen (Center for Research in Neuroscience, McGill University, Montreal).

Antibody production. To generate a polyclonal antibody-specific for NHE6, a recombinant fusion protein of glutathione *S*-transferase (GST) and the extreme C-terminal segment of human NHE6 (amino acids 608–669) was constructed by cloning into the BamHI/EcoRI sites of the pGEX-2T vector (GE Healthcare). After sequence verification, the plasmid was transformed into the Epicurean Coli BL21-Codon Plus strain (Stratagene). Individual colonies were cultured overnight, then diluted at 1:20 in 1 L of bacterial growth media, and further incubated at 37°C to reach sufficient population density. Protein expression was then induced by further incubation with 0.4 mM isopropyl-1-thio-β-D-galactopyranoside at 30°C for 3 h. The bacterial cultures were centrifuged and the resulting pellets were resuspended in 30 ml of lysis buffer (0.4 mg/ml lysozyme in standard PBS, pH 7.4, supplemented with protease inhibitors). Bacteria were subsequently lysed by sonication (model 100 Sonic Dismembrator; Fisher) on ice and then cleared by centrifugation at 4°C for 30 min at 13,000 × *g*. After filtration of the resulting supernatant through a 0.45 μm MILLEX-HV syringe-driven filter unit (Millipore), proteins were purified by incubating the bacterial lysates with glutathione-Sepharose beads (GE Healthcare) overnight at 4°C. The purified GST fusion protein bound to glutathione-Sepharose beads was washed six times with PBS, and then eluted with 10 mM glutathione in PBS. The eluted fractions were concentrated using Amicon Ultra centrifugal filter devices with a 10 kDa cutoff (Millipore) at 3000 × *g* for 10 min.

Rabbit immunizations with the aforementioned fusion protein were performed at the McGill Animal Resource Centre (Montreal) using standard Canadian Council on Animal Care (CCAC)-approved protocols. In brief, two rabbits each received a total of four injections of the antigen mixed with Freund's Complete Adjuvant. Each rabbit was pre-bled (to collect the pre-immune serum), and the injections were administered ~3 weeks apart. Ten days after each injection, both rabbits were subjected to bleeds of 6 ml of blood/kg/every 3 weeks. The rabbits were exsanguinated after completion of the fourth bleed. The NHE6 antiserum was antigen purified as follows. The extreme C-terminal region of NHE6 (amino acids 608–669), which was used to generate the antibody, was fused in frame with the maltose binding protein by cloning into the EcoRI/BamHI sites of the pMAL-c2X vector (New England Biolabs). The fusion protein was purified from *Escherichia coli* BL-21 cultures by binding to a 50% slurry of amylose resin (New England Biolabs). The purified fusion protein was run on a 10% SDS-PAGE and then transferred onto a polyvinylidene difluoride (PVDF) membrane (Millipore) overnight. Next day, the membrane strip was incubated with 2 ml of rabbit serum containing the NHE6 antibody at 4°C overnight. After extensive washes with 50 mM TRIS buffer, the antibody was eluted with 50 mM glycine, pH 2.5, for 15 min, neutralized with 2 M TRIS, pH 8.0, and dialyzed overnight at 4°C in PBS. The antiserum was concentrated using Amicon Ultra centrifugal filter devices with 5 kDa cutoff (Millipore), diluted with equal amounts of glycerol and stored at −20°C.

AP-1 and SH-SY5Y cell culture. AP-1 cells (Chinese hamster ovary (CHO) cells devoid of all plasma membrane NHE activity) (Rotin and Grinstein, 1989) were maintained in α-MEM supplemented with 10% FBS, penicillin (100 units/ml), streptomycin (100 μg/ml), and 25 mM $NaHCO_3$, pH 7.4. SH-SY5Y human neuroblastoma cells were cultured in high glucose DMEM supplemented with 10% FBS. All cells were incubated in a humidified atmosphere of 95% air, 5% CO_2 at 37°C.

Transgenic mice. Hippocampal tissue from transgenic mice expressing enhanced GFP (eGFP) in a subset of neurons was used for NHE6 localization experiments. In these animals, eGFP is fused to the membrane-anchoring domain of a palmitoylated mutant of myristoylated alanine-rich C-kinase substrate (MARCKS), expressed under the control of a Thy1.2 promoter cassette. There are 25 distinct lines of these animals, each exhibiting subtly different patterns of eGFP expression in principal neurons (De Paola et al., 2003). Of these lines, L15 and L17 of both male and female mice were selected as they exhibit low but consistent levels of membrane-targeted eGFP (mGFP)-positive cells within area CA1 of the hippocampus. Tissue preparations from these animals are excellent for conducting localization studies using immunofluorescence and are amenable to sequential confocal imaging, with mGFP-labeled neurons enabling analysis of fine neuronal structures and precise protein localization. All culturing methods were performed according to standards of the CCAC-approved protocols.

Mouse primary hippocampal cultures. Primary cultures were prepared from postnatal day (PD) 0–2 L17 transgenic mice. Briefly, animals were killed by decapitation, their brains removed, and hippocampi dissected out. Dissected hippocampi were maintained in chilled HBSS supplemented with 100 μM HEPES buffer and 0.6% glucose, then digested with 165 U papain for 30 min at 37°C. Recovered neurons and glial cells were dissociated by trituration and suspended in DMEM supplemented with 1% penicillin-streptomycin, 10% FBS, and 0.6% glucose. Cells were then plated onto poly-D-lysine-coated 10 mm coverslips at a density of 12,000 cells/cm^2 and placed in an incubator at 37°C. After 24 h, plating media was replaced with neuronal growth media consisting of Neurobasal-A, 2% B-27 supplement, 1% GlutaMAX, and 1% penicillin-streptomycin.

Neurons were fed every 3–4 d, maintained 14+ d *in vitro* (DIV) in a humidified atmosphere of 95% air, 5% CO_2 at 37°C.

Organotypic mouse hippocampal slice cultures. Organotypic hippocampal slice cultures were prepared from PD6–PD8 L15 transgenic mice as previously described (Gähwiler et al., 1997, 1998). Briefly, animals were killed by decapitation, their brains removed, and hippocampi dissected out. Coronal hippocampal slices (300–400 μm) were generated using a McIllwain tissue chopper (Stoelting) and were embedded in a plasma clot on poly-D-lysine-coated (Sigma Aldrich) glass coverslips. Coverslips were transferred to flat-bottomed culture tubes with medium consisting of 25% horse serum, 25% HBSS, and 50% basal medium Eagle. Cultures were allowed to mature for 3, 7, and 21–28 DIV before experimentation. Organotypic cultures maintain intrinsic connectivity, neuronal organization, and physiological characteristics of neurons *in vivo* (Gähwiler et al., 1997; 1998). During the first week of development following explantation, neurons undergo active synaptogenesis (Dailey and Smith, 1996; Fiala et al., 1998). An initial overproduction of synapses onto dendrite shafts and immature dendritic protrusions is followed by a critical period of refinement whereby superfluous connections are eliminated and others are stabilized. During the next 2 weeks in culture, pruning of synapses occurs and the total number of synapses decreases. The density of synaptic connections reaches an equilibrium state that remains stable in cultures maintained 21+ DIV (McKinney, 2010). Our study using this culture system has been performed primarily in area CA1 where neurons receive glutamatergic inputs from area CA3 via the Schaffer collateral axons; these are the most studied synapses in experimental models of learning and memory.

Cryostat sectioning. Neonatal animals (PD6–PD8) were killed by decapitation, their brains removed, and flash-frozen at −30°C in 2-methyl butane. Older animals (3–7 weeks, 4–8 months) were anesthetized with CO_2 before being decapitated, and their brains were frozen in the same manner. Serial transverse sections of the mouse brains (20 μm) were cut on a freezing microtome (Leica) and transferred to gelatin-subbed slides (Southern Biotech), which were kept at −80°C for later immunohistochemical (IHC) processing.

Immunoblot analysis. For Western blot analysis, cells were grown in 10 cm diameter dishes and transiently transfected with 5 μg of plasmid DNA encoding $NHE6_{HA}$ (NHE6 containing the influenza virus HA epitope at its extreme C terminus), using Lipofectamine (Invitrogen) according to the manufacturer's recommended procedure. Forty-eight hours post-transfection, cell lysates were obtained by washing cells twice with ice-cold PBS, followed by scraping in 0.5 ml of lysis buffer (1% Triton X-100; Sigma Aldrich/PBS supplemented with protease inhibitor mixture; Roche Diagnostics). The lysates were incubated for 30 min on a rocker at 4°C, and then centrifuged at 16,000 × *g* for 20 min at 4°C to pellet the nuclei and cellular debris. Ten to 20 μg of protein from the resulting supernatants were eluted in SDS-sample buffer (50 mM Tris-HCl, pH 6.8, 1% SDS, 50 mM dithiothreitol, 10% glycerol, 1% bromophenol blue), and subjected to 10% SDS-PAGE, then transferred to PVDF membranes for Western blotting. The membranes were blocked with 5% nonfat skim milk for 1 h, then incubated with the specified primary antibodies (mouse monoclonal anti-HA 1:5000, rabbit polyclonal anti-NHE6 1:3000, mouse monoclonal anti-transferrin receptor 1:1000, rabbit polyclonal anti-TOM70 1:1500) in 0.1% Tween 20/PBS, followed by extensive washes and incubation with goat anti-mouse or anti-rabbit secondary antibodies conjugated to HRP (1:7500) for 1 h. Immunoreactive bands were detected using ECL Western blotting detection reagents (GE Healthcare).

For knockdown experiments, AP-1 cells stably expressing $NHE6_{HA}$ were plated into 6-well plates and transfected with 100 nM nontargeting siRNA pool#1 or SMARTpool NHE6 small interfering RNA (siRNA; Dharmacon) using Dharmafect1 transfection reagent (Dharmacon) according to the manufacturer's recommended protocol. Seventy-two hours post-transfection, cell lysates were obtained, as mentioned previously. Ten micrograms of protein were separated by SDS-PAGE and subjected to immunoblotting with either our in-house rabbit polyclonal anti-NHE6 antibody (1:3000) or mouse monoclonal anti-β-tubulin antibody (1:10,000).

To examine endogenous expression of NHE6 in brain tissues, commercially available lysates of human whole brain, mouse whole brain (Abcam), and rat cerebrum (BD Biosciences) were used.

Cell fractionation by differential gravity centrifugation. One 10 cm dish of AP-1 cells stably expressing $NHE6_{HA}$ and six plates of SH-SY5Y neuroblastoma cells were grown to confluence. Cells were rinsed twice with ice-cold PBS and one time with 1× Homogenization Buffer (HB) (0.25 M sucrose, 1 mM EDTA, 20 mM HEPES-NaOH, pH 7.4, supplemented with protease inhibitor mixture), then collected in 400 μl HB and lysed by passing 15 times through a 26 gauge needle. One whole adult mouse brain was homogenized mechanically using a 7 ml glass tissue grinder (Wheaton) in 1× HB (100 μl HB/10 mg of tissue), followed by sonication (model 100 Sonic Dismembrator; Fisher).

The lysates were centrifuged at 700 × *g* to remove the nuclei, and the supernatants, representing the S0.7 total lysate fraction, were transferred to fresh Eppendorf tubes. An aliquot of this fraction was removed for Western blot analysis and the rest was centrifuged at 6000 × *g* for 10 min to extract mitochondria (P6 pellet). The remaining supernatant, called the S6 fraction, was transferred to a fresh tube. The P6 fraction was resuspended in 100 μl of 1% Triton X-100/PBS, pH 7.4, by rocking overnight at 4°C. The S6 supernatant was centrifuged at 30,000 × *g* for 30 min to pellet the microsomal fraction (P30 pellet), which was then solubilized in 100 μl of 1% Triton X-100/PBS, pH 7.4, by rocking overnight at 4°C. The remaining S30 supernatant was centrifuged at 100,000 × *g* for 45 min to sediment the lighter plasma membrane fraction (P100). The P100 pellet was solubilized in 50 μl of 1% Triton X-100/PBS, pH 7.4, by rocking overnight at 4°C. Samples of the resulting fractions (S0.7, P6, P30, and P100) were resolved by SDS-PAGE and immunoblot analysis using the affinity-purified rabbit polyclonal NHE6 antibody (1:1000), followed by incubation with a goat anti-rabbit-HRP-conjugated secondary antibody (1:5000). Immunoreactive bands were detected using Western Lightning Plus-ECL reagents (PerkinElmer).

Immunofluorescence. SH-SY5Y cells were grown on glass coverslips coated with 2 μg/ml fibronectin (Sigma). To examine the subcellular localization of NHE6, cells were fixed in 2% paraformaldehyde (PFA)/PBS for 20 min at room temperature, permeabilized with 0.1% saponin/PBS for 20 min, and then blocked in 10% goat serum/0.01% saponin/PBS for 1 h at room temperature. Cells were subsequently incubated with the specified primary antibodies (mouse monoclonal anti-transferrin receptor 1:200 or rabbit polyclonal anti-NHE6 1:500) overnight at 4°C. The next day, cells were washed four times with 10% goat serum/0.01% saponin/PBS, and then incubated with Alexa Fluor 568- or Alexa Fluor 488-conjugated secondary antibodies at a dilution of 1:2000 in 10% goat serum/0.01% saponin/PBS for 1 h at room temperature. After extensive washes with PBS, coverslips were mounted onto glass slides with Aqua Poly/Mount mounting medium (Polysciences).

Organotypic hippocampal slice cultures were fixed with 4% PFA/0.1 M PB, pH 7.4 (Sigma Aldrich), overnight at 4°C, and washed with 0.1 M PB, pH 7.4. Cultures were pre-incubated overnight at 4°C in blocking buffer consisting of 0.8% Triton X-100/3% heat-inactivated horse serum (HIHS)/0.1 M PB. Cultures were then treated with our primary polyclonal anti-NHE6 (1:250) in 0.4% Triton X-100/1.5% HIHS/0.1 M PB for 5 d at 4°C, before being washed with 1.5% HIHS/0.1 M PB. Cultures were incubated with Alexa Fluor 594 secondary antibody (1:250) in 1.5% HIHS/0.1 M PB for 2 h at room temperature, before final washing steps with 1.5% HIHS/0.1 M PB.

Cryostat sections were fixed in 4% PFA/PB for 20 min at room temperature and washed in 0.1 M PB. Sections were permeabilized for 15 min in 0.4% Triton X-100/1.5% HIHS/0.1 M PB before incubating in our primary polyclonal anti-NHE6 (1:250) diluted in permeabilizing solution for 48 h at 4°C. Sections were washed in 1.5% HIHS/0.1 M PB before incubation with Alexa Fluor 594 secondary antibody (1:250) in the same buffer for 20 min at room temperature before a final washing step with 1.5% HIHS/0.1 M PB.

For colocalization studies, primary hippocampal cultures were fixed with 4% PFA/0.1 M PB for 15 min at room temperature, washed, and then permeabilized for 1 min in 0.2% Triton X-100/0.1 M PB. Neurons were then blocked for 1 h at room temperature in 0.2% Triton X-100/1% HIHS/0.1 M PB, before being incubated with primary antibodies (NHE6

1:1000, Stx-13 1:500, EEA1 1:1000, GluA1 1:200) diluted in blocking solution for 90 min at room temperature. After washing, cells were incubated with a combination of secondary antibodies (Alexa Fluor 594, Alexa Fluor 647, Cy5, Dylight649; 1:1000) in 1% HIHS/0.1 M PB for 30 min at room temperature. For experiments evaluating NHE6 colocalization with soluble transferrin, live primary hippocampal cultures were first incubated with AF-Tfn (100 μg/ml) for 1 h at 37°C to label recycling endosomes, before subsequent processing for immunocytochemistry (ICC).

All processed mouse tissues were mounted onto SuperFrost (Menzel-Glaser) microscope slides using UltraMount fluorescence mounting medium (Dako). Control preparations omitting the primary or secondary antibodies to confirm specificity were processed simultaneously in the same manner (Burry, 2000) according to the protocol for that preparation type.

Glycine-mediated chemical LTP and synaptic insertion of GluA1-containing AMPA receptors. Glycine-mediated chemical long-term potentiation (gly-ChemLTP) was induced in primary hippocampal neurons as previously described (Fortin et al., 2010). Briefly, neurons were mounted into a recording chamber of an upright microscope, continuously perfused for 15 min with normal artificial CSF (nACSF) containing the following (in mM): 125 NaCl, 2.5 KCl, 2 $CaCl_2$, 1 $MgCl_2 \cdot 6H_2O$, 5 HEPES, and 33 D(+)-glucose, pH 7.3, osmolarity 290 mOsmol/L. The nACSF was then replaced with a stimulating solution of Mg^{2+}-deficient ACSF containing the following (in mM): 125 NaCl, 2.5 KCl, 2 $CaCl_2 \cdot 2H_2O$, 5 HEPES, 33 D(+)-glucose, 0.2 glycine, 0.02 (−)-bicuculline methochloride, and 0.003 strychnine hydrochloride. After 10 min at room temperature, neurons were reperfused with nACSF for 20 min. The gly-ChemLTP induction protocol was also repeated in primary cultures that were pretreated with the NMDA glutamate receptor competitive antagonist (RS)-3-(2-carboxypiperazin-4-yl)-propyl-1-phosphonic acid ((RS)-CPP; 50 μM) (Davies et al., 1986) for 15 min before gly-ChemLTP application. The antagonist was also included in the chemical potentiation solution (CPP + gly-ChemLTP). Some preparations that were pretreated with (RS)-CPP were not perfused with chemical potentiation solution, instead they were reperfused with only (RS)-CPP in nASCF before fixation, to control for any effects of this agent alone (CPP + CTRL). Finally, control (CTRL) cultures were continuously perfused with nASCF throughout the entire duration of the experiment. Following experimentation, neurons were immediately fixed in 4% PFA/0.1 M PB and processed for GFP and NHE6 ICC. Coverslips were mounted onto microscope slides using UltraMount fluorescence mounting medium (Dako) for subsequent confocal imaging.

To verify induction of LTP, AMPAR insertion was monitored in non-transgenic primary hippocampal neurons, which were cotransfected with a plasmid containing a GFP-tagged superecliptic pHluorin attached to the AMPAR subunit GluA1 (SEP-GluA1) and an mCherry red cytoplasmic marker, using a high Ca^{2+}-phosphate transfection protocol. This transfection method was performed as previously described (Jiang and Chen, 2006), with some modifications. Briefly, at 10–12 d after plating, coverslips containing cultured neurons were transferred to a 35 mm Petri dish with conditioned culture media. Plasmid DNA (4 μg) was diluted in a $CaCl_2$ solution (250 mM), before being combined with equal parts of a HEPES-buffered phosphate solution (140 mM NaCl, 1.5 mM Na_2HPO_4, 50 mM HEPES, pH 7.05). Neurons were incubated in the DNA-Ca^{2+}-phosphate solution for 1–2 h at 37°C/5% CO_2. Coverslips were washed with 2-(4-morpholino) ethanesulfonic acid (MES) acid buffer (10 mM, pH 5.5) to dissolve Ca^{2+}-phosphate precipitate before being transferred back to their original wells for ≥48 h before experimentation. Once expressed, the pH-sensitive SEP reporter only emits strong fluorescence on the cell surface and SEP-GluA1 forms clusters as endogenous AMPARs at postsynaptic terminals. Stimulus-induced AMPAR insertion following gly-ChemLTP was evaluated by increased SEP-GluA1 fluorescence at dendritic spines of primary neurons after stimulation. Transfected neurons were imaged live; neurons were perfused for 15 min with nACSF, which was switched to stimulating solution at time 0 min (see Fig. 8*F*,*i*) and images were acquired at −5 min, 0 min, +10 min (end ChemLTP), and up to +45 min at 5 min intervals relative to stimulation initiation.

Confocal microscopy. AP-1 and SH-SY5Y cells processed for immunofluorescence were examined by laser scanning confocal microscopy using a Zeiss LSM 510 Meta, and images were analyzed using LSM software and Corel CorelDraw version 13. Immunofluorescence preparations of mouse brain tissue were examined using a Leica SP2 confocal microscope, with images acquired using 40× and 63× HCXPL APO oil-immersion objectives (NAs 1.25 and 1.4, respectively). mGFP was imaged using a 488 nm Ar laser line; Alexa Fluor 594 and Alexa Fluor 568 were imaged using a 543 nm HeNe laser line; and Alexa Fluor 647, Cy5, and Dylight649 were imaged using the 633 nm HeNe laser line. Channels were acquired sequentially to prevent spectral overlap of fluorophores. Optical sections of 250–500 nm were taken; frame averaged 3× at low resolution or line-averaged 2× at high resolution, to improve the signal-to-noise ratio. Transfected neurons were imaged live using the same Leica SP2 confocal microscope, images acquired with a 63× water-immersion long working distance lens (HCX APO L U-V-I; NA 0.9). SEP-GluA1 was imaged using a 488 nm Ar laser line and mCherry was imaged using a 543 nm HeNe laser line. Channels were acquired sequentially to prevent bleed-through of fluorophores. Optical sections of 300 nm were taken, line-averaged 2× to improve the signal-to-noise ratio. All image stacks were deconvolved using Huygens Essential software by using a full maximum likelihood extrapolation algorithm (Scientific Volume Imaging) and 3D images were compiled as maximum intensity projections using Imaris software (Bitplane AG).

Electron microscopy of mouse brain. C57BL/16xCD1WT mice were anesthetized with Equithesin (6.5 mg chloral hydrate and 3 mg sodium pentobarbital in a volume of 0.3 ml, and 0.01 ml of heparin (10 USP/ml), i.p., per 100 g body weight). After a quick vascular rinse with 0.1% $NaNO_2$, animals were transcardially perfused with 4% PFA/0.1% glutaraldehyde/0.1 M PB, pH 7.4, for 30 min. Perfusion was continued for 30 min with 4% PFA/0.1 M PB and 30 min with 10% sucrose/0.1 M PB. Following tissue extraction, the brains were placed in 30% sucrose/0.1 M PB overnight at 4°C and dissected the next day to obtain prefrontal cortex and hippocampus. Transverse sections (~50 μm thick) were cut on a Vibratome (TPI). Sections were cryoprotected for 1 h in 30% sucrose/10% glycerol/0.1 M PB and 1 h in 30% sucrose/ 20% glycerol/0.1 M PB. Three freeze-thaw cycles were performed in isopentane precooled in liquid nitrogen. Sections were treated with 1% sodium borohydride, washed, blocked with 0.5% bovine serum albumin (BSA)/0.1 M PB and treated with our rabbit polyclonal anti-NHE6 antibody (1:200) in 0.1% BSA/0.1 M PB overnight at 4°C. After washes, sections were incubated with 0.8 nm gold-conjugated goat anti-rabbit secondary antibody (1:50; Cedarlane) in 0.1% BSA/0.1 M PB. The signal was amplified using a silver intensification kit (GE Healthcare). All sections were then incubated for 1 h in 1% osmium tetroxide/0.1 M PB at 4°C. Following dehydration in ascending concentrations of alcohols and propylene oxide, the sections were flat embedded in Epon resin. After polymerization, the blocks were trimmed to isolate the CA3 and CA1 regions of the hippocampus. Ultrathin sections were cut on a Reichert–Jung ultramicrotome using a diamond knife. The ultrathin sections were collected onto one-slot, formvar-coated grids, counterstained with uranyl acetate and lead citrate, and examined with a Philips 410 electron microscope equipped with a digital camera (Philips Electron Optics). The experimenters were blinded to treatment for analyses.

Measurements and quantifications. For NHE6 immunofluorescence quantification in cryostat and organotypic hippocampal slices (see Fig. 4*C*,*D*), all 3D stacks were obtained using a Leica SP2 confocal microscope at identical laser intensities, objective, zoom, offset, and gain on the photomultiplier. Single optical sections were selected for analysis at 1/2 and 1/3 depth position in confocal *Z*-series of area CA1 in cryostat-sectioned brain slices and organotypic hippocampal slice cultures, respectively, which had been processed for NHE6 IHC. Mean fluorescent intensity (MFI) was measured across the field of view (512 × 512 pixels) using ImageJ (Rasband, 1997–2008). MFI values were normalized to baseline fluorescence from the earliest time point measured, i.e., PD8 in cryostat slices and 3 DIV in organotypic slice cultures. Statistics were applied to compare fluorescence for immunostained preparations from cryostat-sectioned and organotypic hippocampal preparations, time points of PD8, 21, and 112 and 3, 7, and 21–28 DIV, respectively. The

experimenters were blinded to the developmental time point for analyses.

To determine the spatial localization of NHE6 and its colocalization with EEA1, Stx-13, internalized AF-Tfn, or GluA1 in hippocampal neurons or astrocytes, 3D reconstructions of mGFP-positive structures processed for IHC/ICC were made using Imaris software. Creating an isosurface from the digitized data channel corresponding to mGFP-labeled neurons or astrocytes allowed selection of this region of interest as a masking area for analysis, thus excluding staining not confined to mGFP-positive structures. Analysis of colocalization of proteins of interest within mGFP-positive cells was performed using the ImarisColoc algorithm that generated a new channel (coloc) containing only voxels representing colocalization results, i.e., pixels of channel overlap. Using the spot detection mode in Imaris in conjunction with the generated coloc channel allowed us to track protein localization at dendritic spines and axon terminals. Dendritic spine subtypes in mGFP-positive CA1 pyramidal or primary hippocampal neurons were defined morphologically as stubby, mushroom, and thin, as previously described (Harris, 1992; Sorra and Harris, 2000; McKinney, 2010). Axon terminals were defined as small swellings along the length of mGFP-positive axons. Dendritic spines and terminals were counted as "positive" if the spot-marked protein of interest was within or at a distance of ≤ 0.5 μm from that structure. Protein localization within dendritic spines was further classified as previously described (Park et al., 2006). Immunopositive spots that were within or at a distance of ≤ 0.5 μm from a dendritic spine were categorized to different subspine regions, namely at the base (a), in the neck (b), and/or in the spine head (c). An individual spine could be included in more than one category if proteins of interest were detected in more than one subspine region. The proportion of spines showing NHE6 localization to a given region, or exhibiting NHE6 colocalization with EEA1, AF-Tfn, or Stx-13, was quantified. In organotypic slice cultures, this quantification was initially performed separately in apical and basal dendritic regions; since no significant difference was detected, the data were subsequently pooled. The same data processing and quantification methods were also performed to analyze activity-dependent changes in NHE6 localization in ChemLTP experiments. All analyses were performed blindly so as not to introduce bias. For dual labeling experiments (e.g., NHE6-GluA1), after sequential imaging individual color channels were isolated after masking within the mGFP isosurface, and an outline of the dendrite was drawn and superimposed using Adobe Illustrator CS6.

Specific overlap between NHE6 and GluA1, EEA1, AF-Tfn, or Stx-13 was quantified using the Intensity Correlation Analysis plug-in in ImageJ. Monochromatic maximum intensity projection images were generated in Imaris, after splitting the original Leica files into individual channels representing the distribution of each molecule of interest, as masked inside mGFP-positive neurons. These images were imported into ImageJ and first converted into 8-bit, before a region of interest of dendrite was selected and background was subtracted from this region (default setting of 2 SDs). After running the ImageJ correlation plug-in, the generated Mander's coefficient M1–M2 described to what degree one channel overlaps with the other channel, and vice versa.

Statistical analysis. Unless otherwise stated, error bars indicate SEM and statistical analysis was performed by using the Student's *t* test.

Results

In adult humans, expression of NHE6 mRNA is highest in brain, skeletal muscle, and heart, but is also detected at lower levels in most other tissues (Numata et al., 1998). Similarly, in adult mice, NHE6 mRNA is widely expressed, but is particularly abundant throughout the CNS (Lein et al., 2007) (see also Allen Brain Atlas, http://www.brain-map.org/ and The Jackson Laboratory, http://www.informatics.jax.org/). Despite its broad tissue distribution, mutations in NHE6 cause a pronounced neurological phenotype; severe mental retardation and autistic behavior in humans (Gilfillan et al., 2008; Garbern et al., 2010; Takahashi et al., 2011); and cerebellar degeneration and motor hyperactivity in mice (Strømme et al., 2011), indicative of a critical role for this transporter in CNS function. Earlier light microscopy studies using heterologous cell expression systems revealed that exogenous NHE6 localizes to a perinuclear recycling endosomal compartment (Brett et al., 2002; Nakamura et al., 2005; Ohgaki et al., 2008). However, information regarding its precise localization and function in the brain is lacking, yet essential to gain a better understanding of its role in nervous system function.

To this end, we developed an isoform-specific rabbit polyclonal antibody using recombinant fusion proteins comprised of bacterial GST linked to a unique C-terminal segment of human NHE6 (amino acids 608–669 or 640–701 of the NHE6-v0 or NHE6-v1 splice-variants, respectively) as antigen. To demonstrate specificity of the affinity-purified NHE6 antibody, a chemically mutagenized CHO AP-1 cell line that lacks expression of plasmalemmal NHE1 as well as other plasma membrane-type NHEs (i.e., NHE2–NHE5) (Rotin and Grinstein, 1989) was transiently transfected individually with HA epitope-tagged forms of rat NHE1 (i.e., a representative of the plasma membrane-type NHEs), human NHE6, or its more closely related paralogs human NHE7–9. Following a 48 h incubation period, cell lysates were prepared and analyzed by Western blotting. As shown in Figure 1*A*, left, two strong immunoreactive signals were detected for $NHE6_{HA}$; a slower migrating, fully glycosylated form (~82–90 kDa) and a faster migrating core-glycosylated form (~65 kDa) that correspond to the expected sizes of $NHE6_{HA}$. These bands were not seen in lysates of cells that were untransfected or transfected with other isoforms, thereby confirming the selectivity of the antibody for NHE6. As a control, the blots were subsequently stripped and reprobed with an anti-HA monoclonal antibody to verify the expression of the NHE isoforms (Fig. 1*A*, right). It is noteworthy that the antibody did not detect native hamster NHE6 in cell lysates of untransfected AP-1 cells, despite the fact that they readily recognize the corresponding isoforms in whole brain homogenates from other rodents such as rats and mice (Fig. 1*D*). This may reflect low levels of expression that are below the detection threshold of our antibody or species sequence differences that we cannot yet ascertain as the genomic/mRNA sequences for hamster NHE6 are unknown. To address the former point, various crude membrane fractions were prepared from untransfected AP-1 cells using differential gravity centrifugation. The results showed that the antibody did not detect native NHE6 in AP-1 cells, despite the enrichment of membrane fractions that contain recycling endosomes (data not shown). Thus, while species differences cannot be discounted, the data suggest that expression of native NHE6 might be extremely low or absent in this cell line. To further examine the specificity of the NHE6 antibody and its ability to detect native NHE6 in cells, additional subcellular fractionation and immunoblot analyses were performed using AP-1 cells that stably express human $NHE6_{HA}$ (as a positive control), human neuroblastoma SH-SY5Y cells, and mouse whole-brain homogenates. NHE6 was detected in all examined fractions of the various cells/tissues, but was enriched in the microsomal (P30) and plasma membrane (P100) fractions relative to the more dense mitochondrial fraction (P6) (Fig. 1*B*). To confirm the specificity of the NHE6 antibody, a parallel gel was run and immunoblotted with the antibody pre-incubated with competing immunizing antigen. As shown in Figure 1*B*, immunodetection of NHE6 was effectively blocked under these experimental conditions, confirming the selectivity of the signal obtained with the NHE6 antibody. The identity of the different fractions was confirmed by immunoblotting with antibodies that recognize various established compartment markers; i.e., the Tf-R, which is enriched in the endosomal

P30 and the plasma membrane P100 fractions and TOM70, which is enriched in the P6 mitochondrial fraction. As a final test to validate the NHE6 antibody, human NHE6 expression was knocked down using siRNA in stably expressing AP-1/$NHE6_{HA}$ cells and then examined by immunoblot analysis. As shown in Figure 1*C*, top, the abundance of NHE6 protein was significantly reduced in cells treated with the specific anti-NHE6 siRNA when compared with control cells treated with a scrambled, nontargeting siRNA. To eliminate the possibility that the knockdown observed in the presence of the anti-NHE6 siRNA is due to nonspecific effects, a parallel gel was loaded with the same samples and immunoblotted with anti-tubulin antibody. No difference in tubulin expression was detected in cells treated with scrambled versus anti-NHE6 siRNA (Fig. 1*C*, bottom).

To examine the utility of our antibody to detect NHE6 expression across different species, homogenates of rat cerebrum, human and mouse whole-brain, and isolated mouse hippocampus were fractionated by SDS-PAGE and immunoblotted with the native NHE6 antibody. As shown in Figure 1*D*, both the core- and fully glycosylated forms of NHE6 were detected in all examined tissues. Lysates of AP-1 cells transfected with empty vector and the tagged $NHE6_{HA}$ form were resolved on the same blot as negative and positive controls, respectively. The observation that our antibody can recognize not only human, but also mouse and rat NHE6, highlights the utility of this probe for further analysis of NHE6 expression in brains from different animal models.

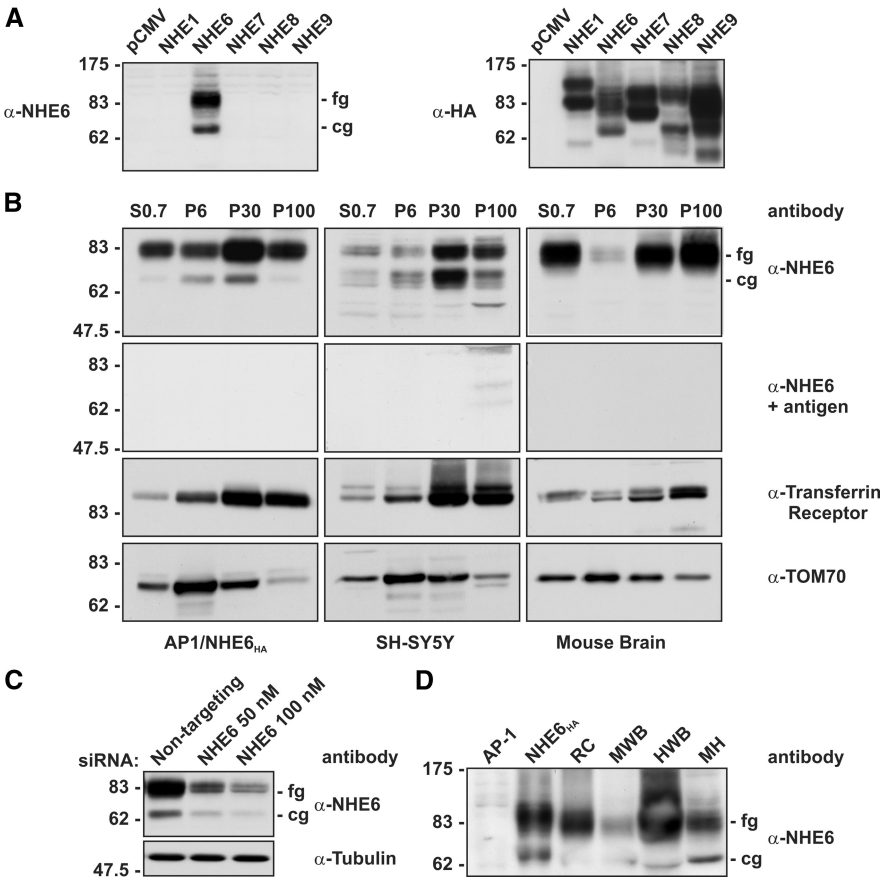

Figure 1. Characterization of an NHE6 isoform-specific rabbit polyclonal antibody by immunoblotting. ***A***, Lysates of AP-1 cells transiently expressing rat $NHE1_{HA}$, human $NHE6_{HA}$, $NHE7_{HA}$, $NHE8_{HA}$, and $NHE9_{HA}$ were subjected to SDS-PAGE and immunoblot analysis. When the blot was probed with the affinity-purified anti-NHE6 antibody (α-NHE6), a signal was detected only in cells transfected with $NHE6_{HA}$ (left). The immunoblot was reprobed with a mouse monoclonal anti-HA antibody (α-HA), showing expression of all NHE isoforms (right). ***B***, Homogenates of AP-1/$NHE6_{HA}$ cells, SH-SY5Y cells, and mouse whole-brain were fractionated by differential gravity centrifugation to enrich for the following subcellular compartments: S0.7 (total cell supernatant lacking nuclei), P6 (mitochondria), P30 (microsomes), and P100 (plasma membrane) (see Materials and Methods for details), followed by SDS-PAGE and immunoblot analysis with the anti-NHE6 antibody. NHE6 was enriched in the P30 microsomal and P100 plasma membrane fractions. When the NHE6 antibody was pre-incubated with the immunizing antigen, no bands were detected. The membranes were also immunoblotted with antibodies that recognize established compartment markers; i.e., the Tf-R, which is enriched in the endosomal P30 and the plasma membrane P100 fractions, and TOM70, which is enriched in the P6 mitochondrial fraction. ***C***, In AP-1 cells stably expressing human $NHE6_{HA}$, our NHE6 antibody detected reduced expression of NHE6 only in cells treated with the specific anti-NHE6 siRNA and not in cells treated with a scrambled siRNA (top). As a control, tubulin levels were not affected by the depletion of NHE6 by siRNA (bottom). ***D***, Detection of native NHE6 in brain tissue homogenates. Lysates of AP-1 cells transiently transfected with empty vector (AP-1) or $NHE6_{HA}$, as well as homogenates of rat cerebrum (RC), mouse whole-brain (MWB), human whole-brain (HWB), and mouse hippocampus (MH) were subjected to SDS-PAGE and immunoblot analysis with the anti-NHE6 antibody. The fully glycosylated (fg), mature form of NHE6, as well as the core-glycosylated form (cg) are visible.

Detection of native NHE6 by light and electron microscopy

Efficacy of the anti-NHE6 antibody in cellular localization analyses was evaluated initially by dual immunolabeling confocal microscopy in human neuroblastoma SH-SY5Y cells. As shown in Figure 2*A*, immunoreactive signals for native NHE6 were detected in punctate vesicles in the soma and neurites that overlapped significantly with Tf-R-containing endosomes. Additional control experiments showed no detectable signals in SH-SY5Y neuroblastoma cells labeled with the primary NHE6 antibody in the presence of competing immunizing antigen (Fig. 2*B*).

As revealed above by immunoblot analysis (Fig. 1*D*), NHE6 is detected in homogenates of mouse hippocampus. To provide a more refined evaluation of its subcellular distribution, we examined the localization of native NHE6 in the CA1 and CA3 regions of mouse hippocampus by transmission electron microscopy (TEM). As shown in Figure 3, NHE6-positive puncta were detected in dendrites, occasionally adjacent to postsynaptic densities (PSDs), which is suggestive of excitatory synapses. Some NHE6-positive puncta were also occasionally observed in presynaptic terminals (Fig. 3*B*). In control experiments, staining was not observed in the absence of primary antibody (Fig. 3*A*), confirming the specificity of the signal produced by the NHE6 antibody.

Expression of NHE6 is increased in mouse hippocampus during synaptogenesis

As mentioned earlier, mutations in NHE6 lead to severe developmental delays characterized by intellectual disability, autistic behavior, absence of speech, ataxia, epilepsy, and microcephaly. Hence, to gain a better temporal perspective of its potential contributions to CNS maturation, we examined the developmental expression of NHE6 with a specific focus on the CA1 region of the hippocampus due to its critical role in learning and memory and

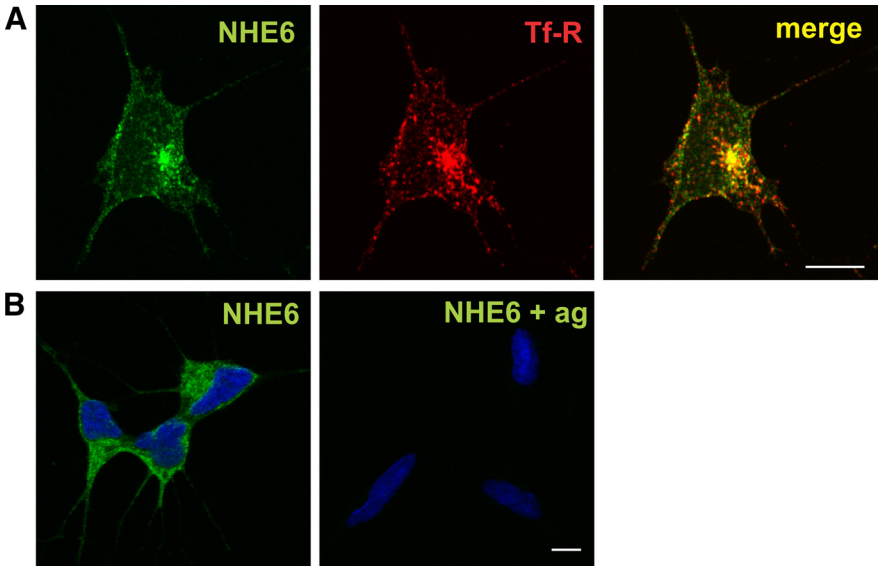

Figure 2. Characterization of an NHE6 isoform-specific rabbit polyclonal antibody by ICC. ***A***, Colocalization of native NHE6 with the Tf-R in the soma and neurites of cultured human SH-SY5Y neuroblastoma cells. Scale bar, 5 μm. ***B***, Control experiment showing that the signal detected with the NHE6 antibody is specific in SH-SY5Y neuroblastoma cells, as no fluorescent signal is observed in the presence of immunizing antigen (ag). Nuclei were stained with DAPI. The green Alexa Fluor 488-conjugated secondary goat anti-rabbit antibody was applied to both samples. Scale bar, 10 μm.

because synapse development in this region has been extensively characterized. We considered three distinct phases of growth that are thought to encompass neuronal circuitry development (Yuste and Bonhoeffer, 2004). To this end, cryostat-sectioned mouse brain slices were prepared from early postnatal (8 d), young adult (50 d), and mature animals (3 months of age or older). In addition, the distribution of NHE6 was examined using mouse hippocampal organotypic slice cultures prepared from PD6 animals and maintained *in vitro* for 3, 7, and 21–28 d. An advantage of this latter preparation is the ability to maintain brain tissue in an *in vitro* environment that permits neurons to continue developing following explantation. Organotypic slice cultures maintain intrinsic connectivity, neuronal organization, and physiological characteristics as seen *in vivo* and are readily amenable to experimental manipulation. Furthermore, to define the subcellular distribution of NHE6 at high resolution, hippocampal organotypic slices were isolated from transgenic mice (L15 and L17 lines) expressing enhanced GFP fused to the membrane-anchoring domain of a palmitoylated mutant of MARCKS29 (mGFP) under the transcriptional control of the Thy1 promoter, which labels a subset of CA1 pyramidal neurons as described previously (see Materials and Methods) (Richards et al., 2005). Transgenic expression of mGFP allows for visualization and morphological characterization of axons, dendrites, and fine micromembrane projections such as dendritic spines in individual pyramidal cells with greater precision.

In both *ex vivo* and *in vitro* preparations imaged at low magnification, the expression profiles for NHE6 throughout the strata radiatum, pyramidalis, and oriens of area CA1 during postnatal development were similar (Fig. 4*A*,*B*). NHE6 expression intensified in a subset of CA1 pyramidal cell bodies and neuronal processes at later stages of development, which may be a consequence of activity-dependent modulation.

Temporal changes in NHE6 expression were also detected across area CA1. In cryostat-cut sections (Fig. 4*C*), the expression of NHE6 increased significantly by ~2.5-fold at PD50 compared with normalized baseline fluorescence at PD8 (1.0 a.u. ± 0.069; PD50, 2.5 a.u. ± 0.099; $^*p < 0.05$). This was followed by a decrease in this same area to just above baseline levels by PD112 (1.45 a.u. ± 0.083; $^*p < 0.05$). In parallel, we detected a similar increase of NHE6 levels in area CA1 of organotypic slice cultures during *in vitro* development (Fig. 4*D*); by 7 DIV, fluorescence intensity in area CA1 increased by 3.5-fold compared with normalized baseline at 3 DIV (3 DIV, 1.0 a.u. ± 0.28; 7 DIV, 3.6 a.u. ± 0.83; $^*p < 0.05$). However, unlike the *ex vivo* hippocampal sections from older animals, expression in the organotypic cultures did not show an equivalent decrease at later stages of *in vitro* development (21+ DIV, 3.8 a.u. ± 1.10). This plateau effect may be explained by the lack of afferent inputs into the hippocampal formation in slice cultures and thus differential activation patterns in area CA1.

NHE6 localizes in somatodendritic and axonal compartments of hippocampal neurons as well as astrocytes

To examine the subcellular distribution of NHE6 in greater detail, we imaged individual CA1 pyramidal neurons and glial cells at higher magnification, a subset of which could be readily identified in organotypic slice cultures by their mGFP expression (Fig. 5*A*,*B*). Previous studies have shown that at early postnatal stages, CA1 pyramidal cells possess a limited number of fine filopodia and small membrane protrusions along their growing dendrites that correspond to the initial stages of synaptogenesis (Dailey and Smith, 1996; Fiala et al., 1998). By comparison, in the adult brain as well as mature organotypic preparations (21+ DIV) (Fig. 5*C*), CA1 pyramidal neurons have developed a higher density and variable assortment of dendritic spines, morphologically classified as stubby, thin, or mushroom, that serve as the postsynaptic compartment of excitatory connections. As shown in Figure 5, *C* and *E*, NHE6 puncta were detected at the base, neck, and/or head of developing dendritic spines of mGFP-positive CA1 pyramidal neurons. By 21+ DIV, NHE6 was distributed throughout the somatodendritic compartment of CA1 pyramidal neurons in punctate clusters (Fig. 5*C*,*E*). Quantitative analysis indicated that NHE6-positive puncta were present at 85% of dendritic spines in neurons 21+ DIV, most frequently at the spine base and/or head (Fig. 5*E*; base (a), neck (b), head (c), see schematic; a/b/c, 85.00 ± 1.48%; base, 64.01 ± 2.81%; head, 15.82 ± 49.83 ± 3.88%). In addition, NHE6 puncta were detected at ~60% of putative presynaptic terminals in CA1 pyramidal cell axons (Fig. 5*D*,*F*; 58.78 ± 4.366%). The high degree of localization of NHE6 to dendritic spines and axon terminals suggests that this protein may play a role in both excitatory presynaptic and postsynaptic function. Furthermore, NHE6 expression is not only restricted to neurons, as we also detected the presence of NHE6 in punctate clusters in some of the cytoplasmic processes of mGFP-labeled protoplasmic astrocytes (Fig. 5*B*).

NHE6 colocalizes with compartments along the recycling endosomal pathway at dendritic spines of mouse primary hippocampal neurons

Previous studies (Brett et al., 2002; Nakamura et al., 2005; Ohgaki et al., 2008) using heterologous overexpression systems have

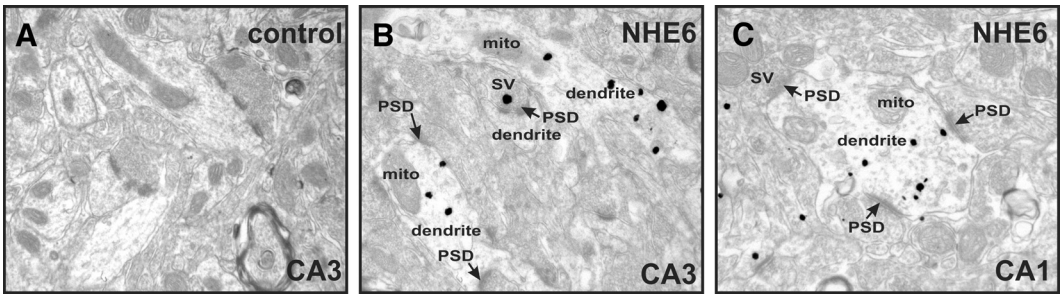

Figure 3. Subcellular localization of native NHE6 in areas CA3 and CA1 of mouse hippocampus by TEM. ***A***, In control experiments, no signals were observed in hippocampal area CA3 in the absence of primary antibody, demonstrating the specificity of the signal produced by the NHE6 antibody. ***B***, NHE6-positive puncta were present mostly in dendrites (sometimes close to PSDs) of hippocampal neurons in area CA3, but are occasionally associated with presynaptic boutons. ***C***, NHE6 immunogold-positive puncta were detected in dendrites in hippocampal area CA1. Magnification: ×24400. SV, Synaptic vesicles; PSD, postsynaptic density; mito, mitochondria.

shown that exogenous NHE6 accumulates in the endocytic recycling compartment. Consistent with this observation, in Figure 2 we showed that endogenous NHE6 also accumulates primarily in Tf-R-containing recycling endosomes in human neuroblastoma cells (Fig. 2*A*). Although such immortalized cell lines retain many exocytic and endocytic sorting mechanisms that are analogous to the more specialized membrane trafficking pathways found in polarized cells such as epithelia and neurons (Cameron et al., 1991; Morimoto et al., 1995; Chavez et al., 1996; Coorssen et al., 1996; Yoshimori et al., 1996; Wilson and Colton, 1997), sorting of NHE6 in these cell lines may differ from that in primary neuronal cells. For example, the synaptic vesicle protein synaptophysin, which colocalizes with Tf-R-associated recycling endosomes when ectopically expressed in CHO cells (Cameron et al., 1991), only partially coincides with Tf-R in the somatodendritic region of hippocampal neurons and is selectively enriched in axonal synaptic vesicles that are devoid of Tf-R (Mundigl et al., 1993). Hence, it is conceivable that NHE6 may sort to discrete vesicular compartments in neuronal cells other than Tf-R-associated endosomes, and this merits further investigation.

To investigate the vesicular nature of the NHE6-positive puncta, dual immunolabeling experiments were performed with established markers for early or sorting endosomes (i.e., EEA1) and recycling endosomes (i.e., syntaxin-12/13, Stx-13, and AF-Tfn). Stx-13 is a member of the SNARE family that is found primarily in tubular early and recycling endosomes of most cells, including hippocampal neurons, where it highly colocalizes with the Tf-R (Prekeris et al., 1998). To improve the visual detection of these compartments, primary cultures of mouse hippocampal neurons of 14+ DIV were

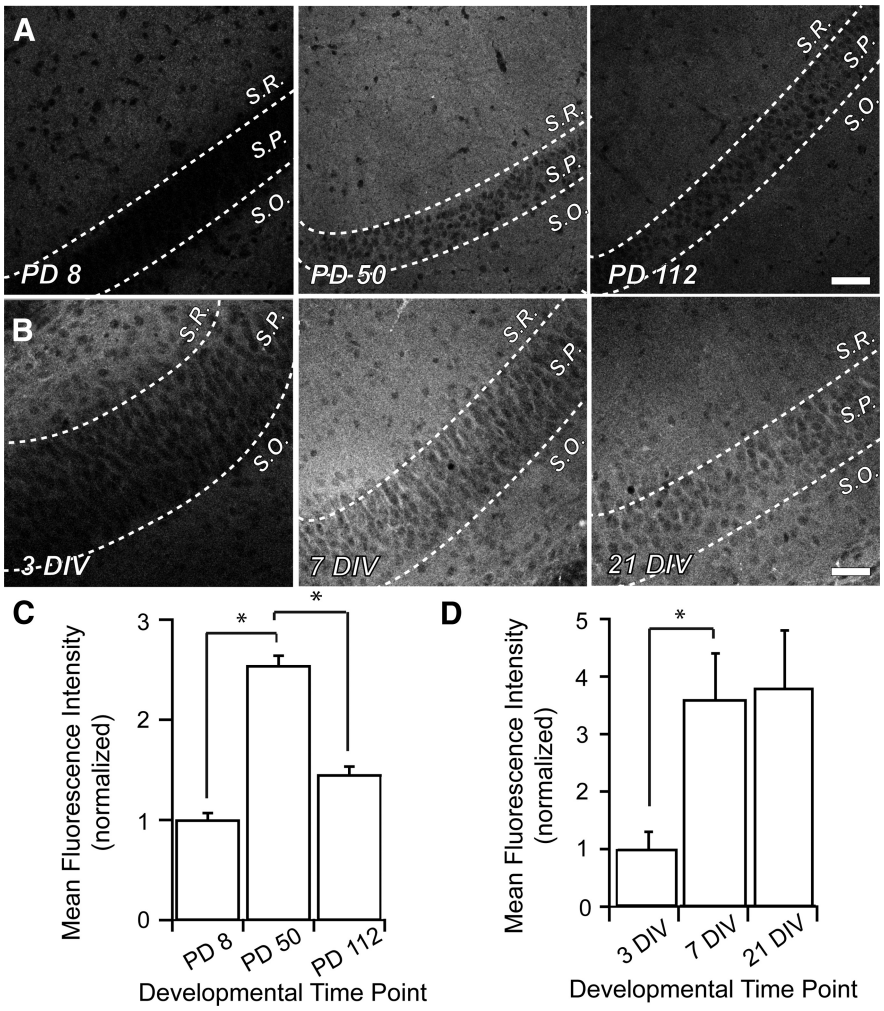

Figure 4. NHE6 is increased in area CA1 of the mouse hippocampus during synaptogenesis. Representative low-magnification confocal micrographs of NHE6 immunostaining in area CA1 of the mouse hippocampus. ***A***, Cryostat-sectioned coronal brain slices from early postnatal (PD8; left), young adult (PD50; middle), and mature animals (PD112; right). During development, NHE6 puncta are diffuse throughout all strata of area CA1. Magnification in all parts (***A***, ***B***) is identical. Scale bar, 50 μm. ***B***, Organotypic mouse hippocampal slice cultures exhibited a similar expression profile as was detected *in vivo*. Throughout slice culture development (3 DIV, left; 7 DIV, middle; 21–28 DIV, right), NHE6 puncta are diffuse throughout all strata of area CA1. ***C***, NHE6 significantly increases by 2.5-fold in area CA1 between PD8 and PD50 as measured by MFI. This period has been shown to be critical for elimination of superfluous connections in the brain and establishing refined synaptic circuits. There is also a significant decrease of NHE6 in area CA1 to ~1.5× of early postnatal levels by PD112, by which time circuitry in the brain has stabilized. $n = 5$ slices for each time point; normalized MFI ± SEM. *$p < 0.05$ by Student's *t* test. ***D***, NHE6, as measured by MFI, significantly increases in area CA1 during the period of synaptic pruning and refinement in organotypic hippocampal slice cultures, but does not return to early postnatal levels. $n = 8$ slices for each time point; normalized MFI ± SEM. *$p < 0.05$ by Student's *t* test. S.R., Stratum radiatum; S.P., stratum pyramidalis; S.O., stratum oriens; PD, postnatal day.

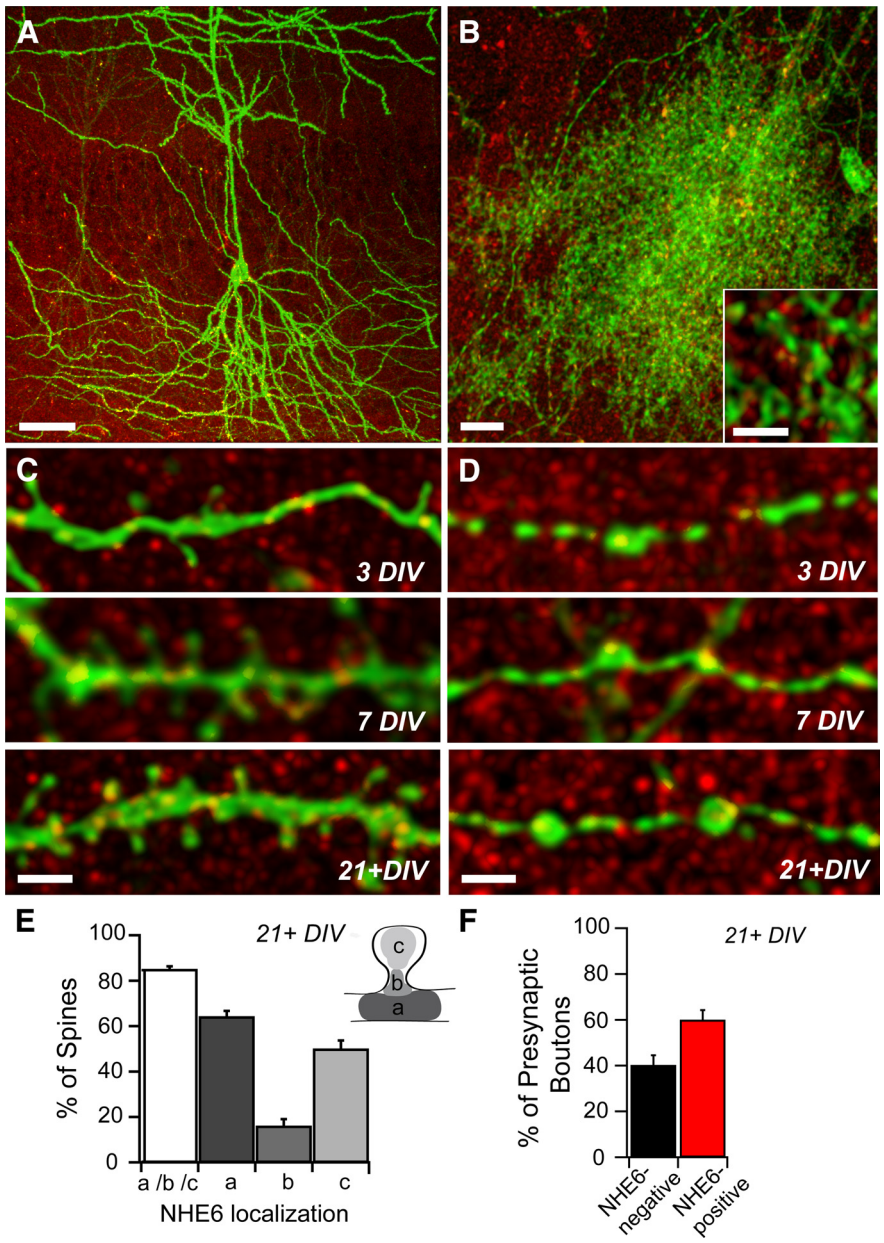

Figure 5. NHE6 localizes to somatodendritic and axonal compartments of hippocampal neurons in mouse organotypic slice cultures. ***A***, Representative confocal micrograph of area CA1 in an organotypic mouse hippocampal slice culture (21+ DIV) processed for NHE6 immunofluorescence. A subset of CA1 pyramidal neurons express mGFP demonstrating complex arborization. NHE6 is found throughout all strata of area CA1 in mature cultures in diffuse puncta, intensified in a subset of pyramidal cell bodies and neuronal processes. Scale bar, 50 μm. ***B***, mGFP-positive astrocyte in area CA1 of a mouse hippocampal slice culture with NHE6 immunolabeling. NHE6 puncta can be seen throughout the cell body and cytoplasmic processes (high-magnification inset) of this glial support cell. mGFP-positive axons from neighboring hippocampal neurons are also visible. Scale bar, 10 μm; inset, 2 μm. ***C***, NHE6 localizes to mGFP-positive CA1 pyramidal cell dendrites and to the base, neck, and head of some dendritic spines during development. During spinogenesis (3 DIV, top), few NHE6 puncta are visible within dendrites and at the tips of growing spines. Increased levels of NHE6 can be found within the dendrite and at the base, neck, and head of dendritic spines as development proceeds (7 DIV, middle; 21+ DIV, bottom). Magnification in all parts is identical. Scale bar, 2 μm. ***D***, NHE6 puncta are visible at a subset of putative presynaptic boutons along mGFP-positive CA1 pyramidal cell axons at all developmental time points. Magnification in all parts is identical. Scale bar, 2 μm. ***E***, Summary of NHE6 localization in mature CA1 pyramidal cell dendrites; inset schematic depicts dendritic spine subregions used for quantification. NHE6 localizes to ~85% of mature dendritic spines, primarily in association with the spine base (a) and/or head (c), and to a lesser extent at the spine neck (b). Note: All-immunopositive spines are described as a/b/c. Percentage values for NHE6 localization at dendritic spine areas (i.e., a, b, and c) do not add up to 100%, as individual spines could fall into more than one category. $n = 326$ dendritic spines along 268.3 μm apical and basal dendrite lengths from eight pyramidal neurons. Mean ± SEM localization per dendrite segment. ***F***, Summary of NHE6 localization in mature CA1 pyramidal cell axons; ~60% of putative synaptic boutons of mature axons show NHE6 localization. $n = 131$ putative presynaptic terminals along 315.2 μm pyramidal cell axon lengths from eight pyramidal neurons. Mean ± SEM localization per axon segment.

established, allowing increased access for molecular manipulations and for live staining procedures (Higgins and Banker, 1998). Like in the organotypic cultures, NHE6 was present in vesicles within the somatodendritic and axonal domains of mGFP-positive hippocampal pyramidal neurons (Fig. 6*A*). Quantitative analysis revealed that NHE6 is associated with ~90% of mature dendritic spines in this system (Fig. 6*F*; 88.51 ± 2.13%; $n = 575$ dendritic spines from 725.01 μm dendrite from 26 neurons).

EEA1 was detected within the somatodendritic compartment of mouse primary hippocampal neurons, where it localized to 47% of dendritic spines (Fig. 6*F*; 52.02 ± 5.17%). This was slightly less frequent than the incidence of AF-Tfn and Stx-13, which were found at ~64 and 69% of mature spines, respectively (AF-Tfn, 64.02 ± 5.06%; Stx-13, 69.56 ± 3.51%). All three markers are found mainly at the dendritic spine base (Fig. 6*F*; EEA1-base, 39.22 ± 3.74%; EEA1-neck, 4.46 ± 1.49%; EEA1-head, 10.28 ± 4.43%; AF-Tfn-base, 48.42 ± 5.29%; AF-Tfn-neck, 8.14 ± 1.47%; AF-Tfn-head, 17.19 ± 2.89%; Stx-13-base, 45.72 ± 3.61%; Stx-13-neck, 4.54 ± 1.39%; Stx-13-head, 14.64 ± 3.67%). Further dual labeling measurements revealed that NHE6 only partially colocalized with these early and recycling endosomal markers; specifically with EEA1 at 35% of dendritic spines (Fig. 6*C*; 34.62 ± 4.10%), with AF-Tfn at 42% of dendritic spines (Fig. 6*D*; 42.02 ± 4.83%) and with Stx-13 at 54% of dendritic spines (Fig. 6*E*; 54.42 ± 4.99%). Puncta of NHE6 were in close proximity to these markers, or partially overlapping, most frequently being found together at the dendritic spine base (Fig. 6*F*; NHE6-EEA1-base, 29.60 ± 4.44%; NHE6-EEA1-neck, 2.59 ± 1.46%; NHE6-EEA1-head, 7.81 ± 3.60%; NHE6-AF-Tfn-base, 34.88 ± 5.09%; NHE6-AF-Tfn-neck, 4.29 ± 1.39%; NHE6-AF-Tfn-head, 12.78 ± 2.49%; NHE6-Stx-13-base, 40.50 ± 4.56%; NHE6-Stx-13-neck, 2.14 ± 1.01%; NHE6-Stx-13-head, 8.49 ± 2.07%). More specifically, by calculating the Mander's coefficient M1–M2, a statistical parameter that describes the degree of channel overlap that is not dependent upon correlated intensity, a clearer picture of the possibility of colocalization of NHE6 and these endosomal markers was revealed. By this measure, ~85% of Stx-13 and 96% of EEA1-positive puncta consistently overlapped with NHE6 ($p < 0.05$), with ~57% of AF-Tfn overlapping with NHE6 ($p < 0.05$). However, a sizable fraction of NHE6 puncta in the dendritic spine heads was

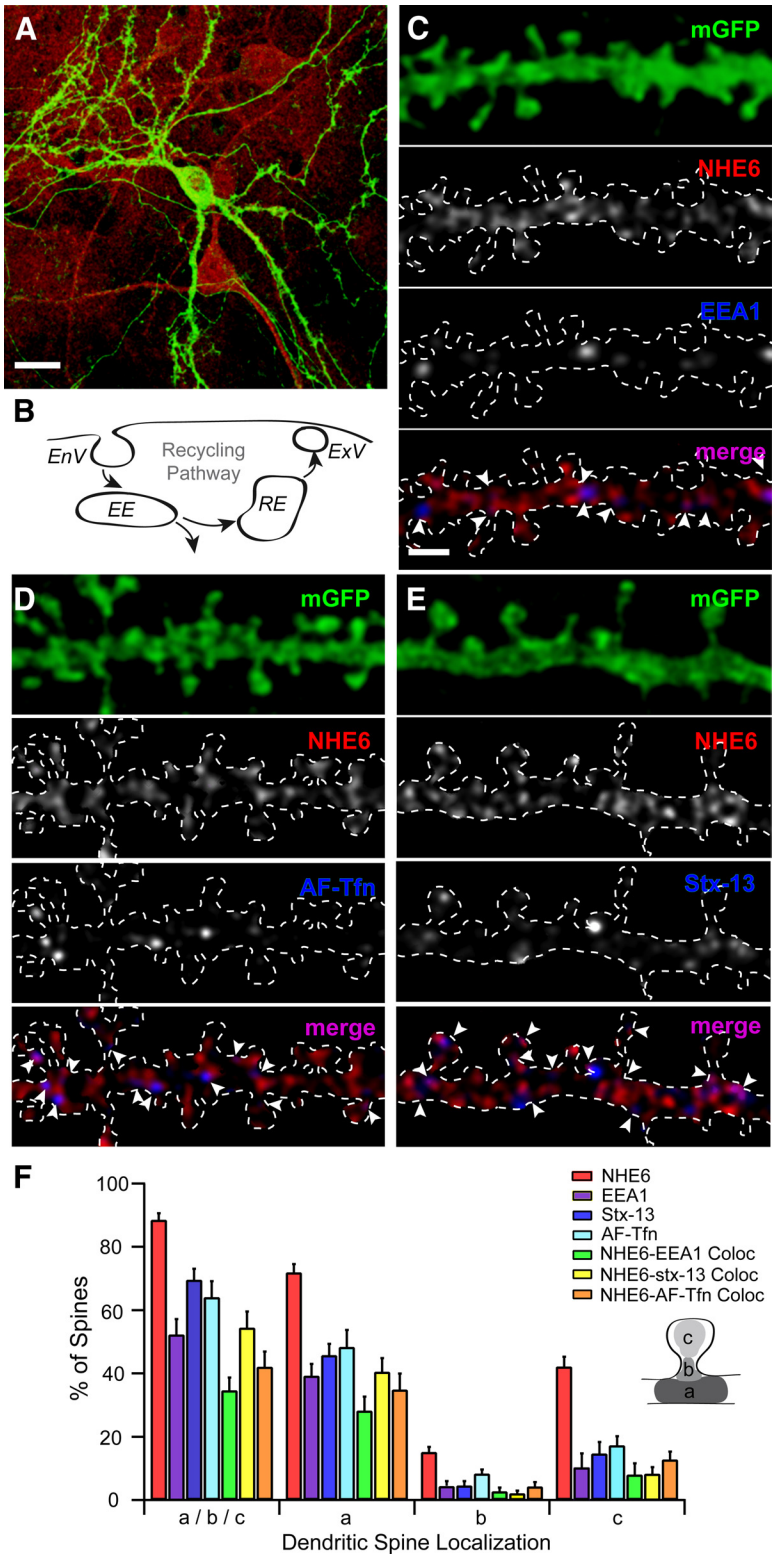

Figure 6. NHE6 colocalizes with early and recycling endosomal markers at dendritic spines of mouse primary hippocampal neurons. ***A***, ***C–E***, Representative confocal micrographs show immunofluorescent localization of NHE6 and its colocalization with early and recycling endosomes positive for EEA1, AF-Tfn, or Stx-13 in mouse primary hippocampal neurons (14+ DIV). Arrowheads denote protein localization at different regions of dendritic spines. ***A***, NHE6 localizes to the somatodendritic compartment of an mGFP-positive neuron. It also localizes to neighboring unlabeled neurons and to cells of the surrounding glial cell bed. Scale bar, 20 μm. ***B***, Simplified schematic representation of the endosomal recycling pathway at the dendritic spine surface. ***C***, NHE6-EEA1 colocalization occurs at a subset of NHE6-positive dendritic spines in primary hippocampal neurons. EEA1 is almost exclusively found in close proximity to or partially overlapping NHE6 puncta. Magnification in all parts (***C–E***) is identical. Scale bar, 2 μm. ***D***, mGFP-positive dendrite following incubation with AF-Tfn (100 μg/ml) for 1 h at 37°C to label recycling endosomes. Puncta of internalized AF-Tfn are frequently adjacent to or overlapping NHE6. ***E***, NHE6-Stx-13 colocalization is seen only at a subset of NHE6-positive dendritic spines in primary hippocampal neurons. Stx-13 is almost exclusively found in close proximity or partially overlapping NHE6 puncta. ***F***, Quantitative summary of NHE6 colocalization with recycling endosomal markers in dendritic spines of primary hippocampal neurons. NHE6 localizes to 90% of mature dendritic spines, showing colocalization with EEA1 at 35% of spines, AF-Tfn at 50% of spines, and with Stx-13 at 40% of spines. By the Mander's coefficient, the majority of Stx-13 and EEA1-positive puncta are significantly overlapped by NHE6 (Stx-13-NHE6: 0.8564, $p < 0.05$; EEA1-NHE6: 0.9611, $p < 0.05$), with approximately half of AF-Tfn overlapping with NHE6 (AF-Tfn-NHE6: 0.5733, $p < 0.05$). NHE6 colocalization with recycling endosomes occurs primarily at the spine base (a) and/or head (c), and to a minimal extent at the spine neck (b) (see inset schematic). Note: All immunopositive spines are described as a/b/c. Percentage values for dendritic spine areas (i.e., a, b, and c) do not add up to 100%, as individual spines could fall into more than one category. $n = 163$ dendritic spines from 172.78 μm dendrite from six neurons, $n_{\text{AF-Tfn}} = 221$ dendritic spines from 228.70 μm dendrite from six neurons, 266 dendritic spines from 323.53 μm dendrite from eight neurons. Mean ± SEM localization per dendrite segment. White dashed line denotes secondary dendrite of an mGFP-positive dendrite. EnV, Endocytic vesicle; EE, early endosome; RE, recycling endosome; ExV, exocytic vesicle; EEA1, early endosome antigen 1; AF-Tfn, Alexa Fluor 568-conjugated transferrin; Stx-13, syntaxin-13; mGFP, membrane-tagged enhanced green fluorescent protein.

seemingly devoid of one or more of these organellar markers, suggesting that NHE6 may be sorted into different pools of recycling vesicles, each presumably containing distinct cargo.

NHE6 significantly overlaps with AMPAR subunit GluA1 in dendrites and dendritic spines of primary hippocampal neurons

Due to its high level of expression at the postsynaptic sites of excitatory pyramidal neurons, we decided to investigate whether NHE6 also colocalizes with other known postsynaptic elements. In particular, we assessed its colocalization with glutamatergic AMPAR subunit GluA1. In the hippocampus, heterotetramers of GluA1-GluA2 and GluA2-GluA3 subunits, with a small contribution from GluA1 homomers, comprise the majority of AMPARs at excitatory synapses. Interestingly, the subunit composition of AMPARs determines their trafficking properties at synapses: receptors that lack GluA1 subunits are constitutively expressed at the synapse, whereas GluA1-containing AMPARs undergo activity-dependent trafficking to and from the postsynaptic membrane (Gerges et al., 2004, 2006; Park et al., 2004; Brown et al., 2007). In mouse primary hippocampal neurons (14+ DIV), we found that NHE6 displayed a high degree of colocalization with the AMPAR subunit GluA1 in dendrites and at dendritic spines (Fig. 7; Mander's

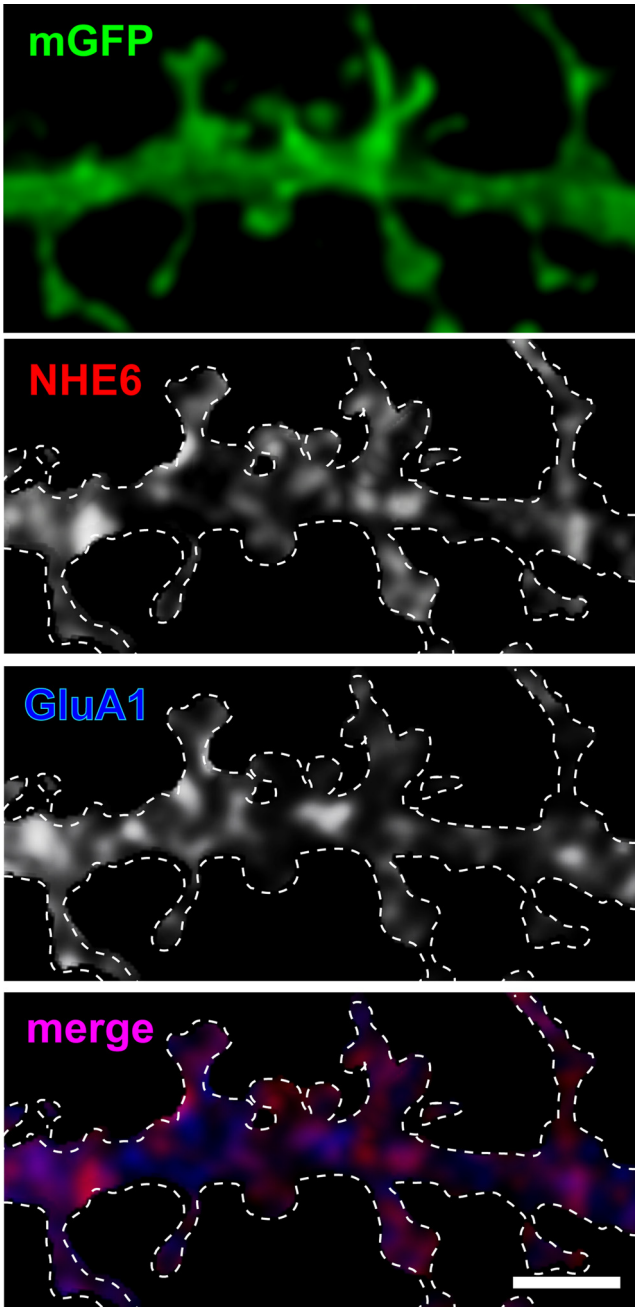

Figure 7. NHE6 significantly overlaps with AMPAR subunit GluA1 in dendrites and dendritic spines of primary hippocampal neurons. Representative confocal micrographs show immunofluorescent localization of NHE6 and GluA1 and their colocalization in mouse primary hippocampal neurons (14+ DIV). NHE6 andGluA1 partially colocalize in dendrites and at dendritic spines, but they are found to be significantly overlapping with one another by the Mander's coefficient (NHE6:GluA1, 0.7916; GluA1:NHE6, 0.845; $p < 0.05$). Magnification in all panels is identical. Scale bar, 2 μm. White dashed line denotes secondary dendrite of an mGFP-positive dendrite.

coefficient: NHE6:GluA1, 0.7916; GluA1:NHE6, 0.845; $p < 0.05$).

NHE6 is increased at dendritic spines following glycine-induced LTP

The detection of NHE6 in EEA1/Stx-13/Tfn-positive recycling endosomes and vesicles containing GluA1 is interesting in light of earlier reports linking these vesicles with the recycling of AMPARs (Lin et al., 2000). Previous studies have shown that at excitatory hippocampal synapses, correlated presynaptic and postsynaptic activity results in a persistent enhancement in synaptic efficacy, widely known as LTP—a phenomenon that has become a cellular paradigm for learning and memory storage in the brain (Malenka and Nicoll, 1999; Lynch, 2004). Delivery of AMPARs to the PSD and new plasma membrane for dendritic spine enlargement during LTP is performed by recycling endosomes (Engert and Bonhoeffer, 1999; Park et al., 2004, 2006; Petrini et al., 2009), which undergo activity-dependent trafficking and are rapidly mobilized to dendritic spines following LTP-inducing stimuli. Hence, using immunofluorescence, we assessed whether the localization of NHE6 is modulated at dendritic spines following the induction of activity.

It is known that eliciting LTP at CA3–CA1 pyramidal cell synapses requires activation of NMDARs and that application of the NMDAR coagonist glycine can induce LTP in cultured mouse brain neurons (Johnson and Ascher, 1987; Lu et al., 2001; Park et al., 2006). In this study, we have used a previously described gly-ChemLTP in primary hippocampal neurons (Fortin et al., 2010). This protocol exhibits many features characteristic of CA1 stimulus-induced LTP and specifically activates NMDARs at synapses receiving spontaneous release of glutamate (Shahi and Baudry, 1993; Lu et al., 2001). We confirmed the efficacy of this protocol to induce LTP at excitatory synapses by expressing a GluA1 construct with an N-terminally fused pH-sensitive GFP, termed SEP, which allowed us to monitor the insertion of AMPARs at the cell surface by visualization of SEP-GluA1 (Fig. 8*F*,*iv*). It is known that synaptic incorporation of GluA1-containing AMPARs is required for stable spine enlargement and long-term synaptic potentiation after plasticity-inducing stimuli (Kopec et al., 2006; Kopec et al., 2007). Indeed, an increase in SEP-GluA1-containing AMPARs was detected at dendritic spines of transfected neurons that received glycine stimulation, as shown in Figure 8*F*,*iv*. Similarly, following gly-ChemLTP, we observed a highly significant increase in NHE6 localization at dendritic spines of primary neurons compared with control (Fig. 8*B*; gly-ChemLTP, 95.65 ± 0.96%; CTRL, 83.90 ± 2.18%; $^{***}p < 0.005$). This effect was blocked by incubation with the potent NMDAR antagonist (RS)-CPP (CPP + gly-ChemLTP; 50 μM; 84.55 ± 1.65%; $^{***}p < 0.005$). The localization of NHE6 following gly-ChemLTP in neurons that were also treated with (RS)-CPP was not significantly different from localization in control untreated neurons ($p = 0.67$). In addition, there were no significant differences in NHE6 localization in neurons that had been treated with (RS)-CPP alone without glycine stimulation compared with control, indicating that the drug itself did not affect NHE6 distribution (data not shown).

NHE6 undergoes redistribution at dendritic spines following glycine-induced LTP

Localization of NHE6 also showed discrete changes at subspine regions (Fig. 8*B*), i.e., there was a significant increase of NHE6 at the base and head of dendritic spines following gly-ChemLTP (CTRL-base, 64.08 ± 2.47%; gly-ChemLTP-base, 74.26 ± 2.98%; CTRL-head, 30.54 ± 4.44%; gly-ChemLTP-head, 43.71 ± 3.28; $^{*}p < 0.05$). The increase in NHE6 at dendritic spine heads following gly-ChemLTP was inhibited in neurons treated with NMDAR blocker (RS)-CPP (CPP + gly-ChemLTP-head, 29.06 ± 3.96%; $^{*}p < 0.05$). Furthermore, we considered whether there were spine type-specific changes in NHE6 localization, as individual spine varieties are known to exhibit differential responses to LTP induction (Kasai et al., 2010). For instance, thin spines are more amenable to plasticity-inducing events and rapidly form or disappear in response to different patterns of synap-

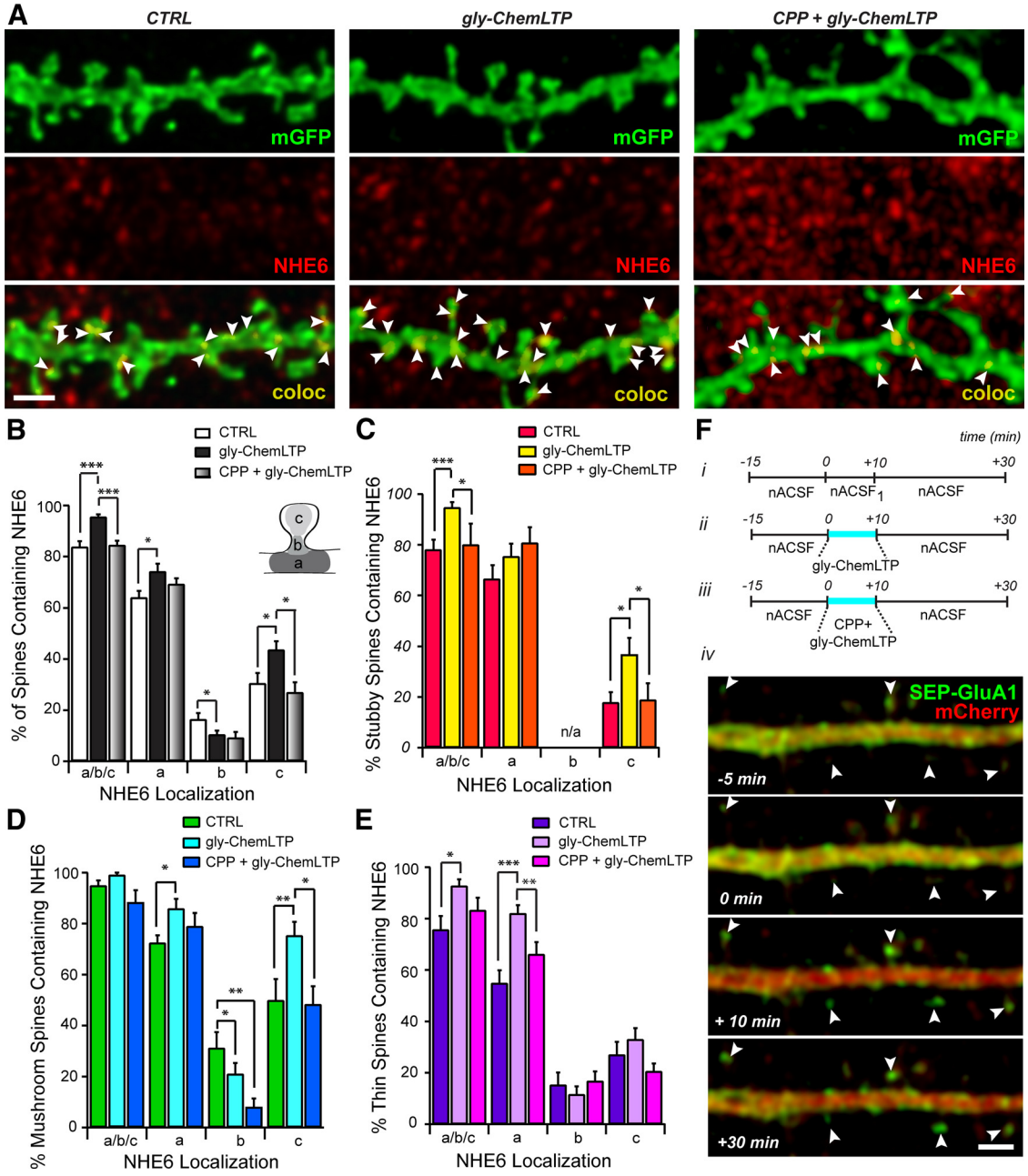

Figure 8. gly-ChemLTP induction leads to changes in NHE6 localization at dendritic spines. ***A***, Representative high-magnification confocal micrographs of mGFP-positive dendrites in untreated (CTRL; left), glycine-treated (gly-ChemLTP; middle), and (RS)-CPP-pretreated/glycine-treated (CPP + glyChemLTP; right) conditions (***F***, ***i-iii***), processed for NHE6 ICC. Arrowheads denote NHE6 localization at different regions of dendrite spines. Magnification in all panels is identical. Scale bar, 2 μm. ***B***, Summary of NHE6 localization at dendritic spines of primary hippocampal neurons in CTRL, gly-ChemLTP, and CPP + glyChemLTP conditions. There is a significant increase in the percentage of mature dendritic spines positive for NHE6 following glycine treatment compared with control and CPP-pretreated neurons. At positive spines, NHE6 is found primarily in association with the spine base (a) and to a lesser extent at the spine head (c) and neck (b) (inset, dendritic spine schematic). NHE6 undergoes a significant increase at the base and heads of dendritic spines, and a significant decrease at the spine neck following glycine application. This effect is inhibited by CPP-mediated NMDAR block. Note: Percentage values for dendritic spine areas (i.e., a, b, and c) do not add up to 100%, as individual spines could fall into more than one category. ***C–E***, Summary of NHE6 localization at dendritic spines of primary hippocampal neurons in CTRL, gly-ChemLTP, and CPP + glyChemLTP conditions according to spine type. Changes in NHE6 localization are specific to individual spine varieties; there are significant increases in NHE6 localization at the base of thin and mushroom spines with glycine treatment, significant decreases at the neck of mushroom-shaped spines, and finally, significant increases at the head of both stubby and mushroom-shaped spines. The increase at mushroom and stubby spine heads is dependent upon NMDAR activation as CPP-pretreatment blocks this effect. Note: All immunopositive spines are described as a/b/c. Stubby spines do not possess distinct neck regions and thus b is indicated as n/a. Percentage values for dendritic spine areas (i.e., a, b, and c) do not add up to 100%, as individual spines could fall into more than one category. $n_{CTRL} = 267$ spines from 264.18 μm dendrite in seven neurons; $n_{gly\text{-}ChemLTP} = 391$ spines from 397.49 μm dendrite in nine neurons; and $n_{CPP + gly\text{-}ChemLTP} = 183$ spines from 225.59 μm dendrite in five neurons. Mean ± SEM localization per dendrite segment. $^{*}p < 0.05$, $^{**}p < 0.01$, $^{***}p < 0.005$ by Student's *t* test. ***F***, ***i-iii***, Experimental paradigms in gly-ChemLTP protocol; CTRL, gly-ChemLTP, and CPP + gly-ChemLTP (see Materials and Methods). ***iv***, Synaptic incorporation of SEP-GluA1-containing AMPARs was detected immediately after gly-ChemLTP (+10 min) and remained stable for up to 20 min after (+30 min) in neurons cotransfected with mCherry and the SEP-GluA1 construct. Arrowheads denote dendritic spines exhibiting GluA1 insertion. Magnification in all parts is identical. Scale bar, 2 μm.

tic activity. In contrast, the morphology of mushroom-shaped spines remains relatively stable over time. Consistent with this notion, the accumulation of NHE6-containing vesicles at stubby and thin spines was increased significantly following potentiation; changes that were prevented by (RS)-CPP (Fig. 8*C*,*E*; Stubby: CTRL, 77.95 ± 4.06%; gly-ChemLTP, 94.74 ± 2.07%; CPP + gly-ChemLTP, 80.05 ± 8.30%; Thin: CTRL, 75.71 ± 5.29%; gly-ChemLTP, 92.73 ± 2.53%; CPP + gly-ChemLTP, 83.29 ± 4.84%). On the one hand, there was no statistically measureable increase in the total number of mushroom-type spines exhibiting NHE6 expression (Fig. 8*D*); however, we detected a prominent redistribution of NHE6 within individual spine types.

The increase in total number of thin spines positive for NHE6 may reflect its recruitment to thin spine bases, as we observed a significant increase of NHE6 localization here following gly-ChemLTP compared with control (Thin: base-gly-ChemLTP, 82.08 ± 3.18%; CTRL, 54.92 ± 4.93%; CPP + gly-ChemLTP, 66.14 ± 4.71%). Interestingly, we found a decrease in NHE6 expression levels at the neck of mushroom-shaped spines, but with a significant increase at their heads (Mushroom: neck-gly-ChemLTP, 19.19 ± 4.24%; neck-CTRL, 35.62 ± 6.20%; head-gly-ChemLTP, 76.96 ± 5.30%; head-CTRL, 49.26 ± 8.33%); this translocation to mushroom spine heads was effectively blocked by treatment with (RS)-CPP (Mushroom head-CPP + gly-ChemLTP, 52.38 ± 7.035%). There was also a significant increase of NHE6 levels at the head of stubby spines, which could account for the increase in overall NHE6 expression at this spine type (Stubby-head: gly-ChemLTP, 36.78 ± 6.52%; CTRL, 17.88 ± 4.07%). The increase at mushroom and stubby spine heads was blocked by (RS)-CPP treatment, again confirming that this effect is NMDAR dependent. However, we did observe some variability in the effectiveness of CPP to block the gly-ChemLTP effect at specific spine regions of individual spine types. For instance, we did not see a significant block of the redistribution of NHE6 at the neck of mushroom spines with CPP pretreatment before chemical LTP. This could be explained by the fact that this is an intermediate region where vesicles are transiting between the base and the spine head in response to activity, but do not actually accumulate there, thereby making it difficult to accurately measure changes in steady-state levels in the neck.

Discussion

Recent studies have linked mutations in human NHE6/*SLC9A6* to pronounced cognitive and developmental impairments characterized by severe intellectual disability, autistic behavior, epilepsy, ataxia, and features closely resembling Angelman and Christianson syndromes (Gilfillan et al., 2008; Garbern et al., 2010; Madrigal et al., 2010; Tzschach et al., 2011). Mice containing a null mutation of NHE6 also display a neurodegenerative phenotype, though less dramatic (Strømme et al., 2011). However, the basis for this phenotype is poorly understood, in part due to the lack of detailed information regarding the molecular and cellular properties of NHE6, especially within the CNS. In this report, we demonstrate that NHE6 protein levels are dynamically regulated during postnatal development in area CA1 of mouse hippocampus where it localizes to both pyramidal neurons and astrocytes. More detailed microscopy analyses of CA1 hippocampal pyramidal neurons revealed that NHE6 resides in vesicles that partially colocalize with known markers of early and recycling endosomes, including vesicles that contain the AMPAR subunit GluA1, and that are noticeably enriched at both excitatory presynaptic terminals and postsynaptic dendritic spines. Significantly, following NMDAR-dependent LTP, NHE6 undergoes a robust recruitment to dendritic spines, alterations that may have important implications for the involvement of NHE6 in learning and memory processes.

While most mammalian organ systems develop primarily during embryogenesis, the CNS undergoes considerable morphological differentiation and acquisition of function during postnatal maturation. We noted a significant and specific increase in NHE6 expression in area CA1 of the hippocampus during the period where spinogenesis and synaptogenesis on hippocampal pyramidal neurons are thought to reach a peak before neuronal circuitry undergoes activity-dependent pruning and refinement (Yuste and Bonhoeffer, 2004). These observations indicate that NHE6-containing vesicles might be involved in establishing appropriate connectivity in the brain. Indeed, we detected the presence of NHE6 at developing dendritic spines as well as excitatory axon terminals during this time frame. Interestingly, maladaptation of spinogenesis and synaptic pruning is correlated with various cognitive disorders such as autism spectrum disorders and fragile X mental retardation syndrome, where affected individuals show alterations in dendritic spine density and maturation (Fiala et al., 2002; Penzes et al., 2011).

The study of dendritic spine maturation and maintenance in hippocampal neurons has implicated the involvement of vesicular trafficking networks (Kennedy and Ehlers, 2006, 2011). In the rat brain, local endosomal compartments have been identified at dendritic spines (Spacek and Harris, 1997; Blanpied et al., 2002; Cooney et al., 2002; Park et al., 2004, 2006; Rácz et al., 2004; Lu et al., 2007; Petrini et al., 2009; Kennedy et al., 2010) and manipulations that acutely disrupt vesicular trafficking in hippocampal neurons cause a rapid decline in dendritic spine size and density, and also block LTP (Park et al., 2006). Previous work in non-neuronal systems has identified a significant role for NHE6 in regulating endocytosis (Xinhan et al., 2011) as well as cell polarity (Ohgaki et al., 2010) in a manner that is dependent on its ability to modulate intravesicular pH. However, the mechanisms linking NHE6 and intravesicular pH to the trafficking machinery of endosomes remain obscure. In the present study, we found that NHE6 partitions predominantly into Tf-R-containing vesicles in SH-SY5Y neuroblastoma cells. NHE6 was also enriched in endosomes located primarily at the base and head of dendritic spines of cultured mouse hippocampal neurons. However, in this case, NHE6 only partially colocalized with classical markers (i.e., EEA1, Tf-R, and Stx-13) of clathrin-mediated recycling vesicles, suggesting that NHE6 may reside in multiple endosomal pools in neurons, each potentially carrying distinct cargo. Indeed, NHE6 was also detected in vesicles containing the AMPAR subunit GluA1. This property could have important implications for its broader involvement in regulating the overall composition of the postsynaptic compartment. Indeed, regulating the composition of the postsynaptic domain by the coordinated trafficking of vesicles containing ion channels, scaffolding molecules, and a variety of signal transduction modulators is required for proper synaptic function. In particular, increasing efforts have been devoted to understanding the precise trafficking of AMPARs, as both acute and long-term alterations in AMPAR localization are critical for synapse formation, maturation, and plasticity.

At glutamatergic synapses, regulation of the number or density of postsynaptic AMPARs defines the synaptic properties of the neuron, as these ligand-gated ion channels are the principle mediators of excitatory neurotransmission (Ehlers, 2000; Roche et al., 2001; Shepherd and Huganir, 2007). Recycling and reinsertion of AMPARs following their activation and internalization at dendritic spines is determined in part by NMDAR activation

(Ehlers, 2000). Following NMDAR-dependent LTP-inducing stimuli, it has been shown that AMPARs are sorted to recycling endosomes, which rapidly mobilize to spine heads to exocytose AMPARs onto the cell surface and provide new lipid membrane for spine expansion (Park et al., 2004, 2006). Our description of the change in NHE6 localization following an NMDAR-dependent chemical LTP makes NHE6 an attractive candidate for involvement in both AMPAR endosomal sorting and recycling. Here, we observed a robust increase in NHE6 at potentiated spines as well as a redistribution of the transporter to dendritic spine heads, which is fitting with the previously observed translocation of recycling endosomes to spine heads during LTP (Park et al., 2004, 2006). Our findings depicting spine type-specific increases in NHE6 at the base of thin and mushroom spines and at the head of stubby and mushroom spines are also interesting because of the differential responsiveness of individual spine varieties to LTP induction (Bourne and Harris, 2007), thus implicating a unique role of NHE6 at different spine types. For instance, thin spines are more amenable to plasticity-inducing events and rapidly form or disappear in response to different patterns of synaptic activity (Holtmaat et al., 2005; Bourne and Harris, 2007). Alternatively, mushroom-shaped spines exhibit relative structural stability over time, which has garnered them a reputation as a substrate for persistent memory formation in the brain (Bourne and Harris, 2007; Matsuo et al., 2008). Furthermore, our detection of NHE6 colocalization with Stx-13, a SNARE protein implicated in directing LTP-induced exocytosis at the spine head, and GluA1 puts it in an appropriate context for involvement in AMPAR recycling (Park et al., 2004, 2006; Kopec et al., 2007). We can only speculate what the redistribution of NHE6 might achieve; however, we suggest that the change in NHE6 localization with NMDAR-mediated chemical LTP could highlight its involvement in postsynaptic plasticity.

Thus far we have only considered a potential postsynaptic role of NHE6. However, NHE6 is also present at the majority of excitatory presynaptic boutons of CA1 pyramidal neurons in mature hippocampal slice cultures. Maintenance of a pH gradient across synaptic vesicles is known to contribute to neurotransmitter loading (Tabb et al., 1992). Interestingly, a recent study has identified an electroneutral nonselective monovalent cation (Na^+, Li^+, or K^+)/H^+ exchange activity in synaptic vesicles that uses the H^+ chemical gradient (ΔpH) generated by the vacuolar H^+-translocating ATPase to mediate the influx of K^+, thereby increasing the membrane potential ($\Delta\psi$) (Goh et al., 2011). The increase in $\Delta\psi$, in turn, stimulates glutamate uptake, effects that are effectively blocked by the NHE-selective pharmacological antagonist 5-(*N*-ethyl-*N*-isopropyl) amiloride (Goh et al., 2011). While the precise molecular identity of this vesicular NHE remains to be established, the presence of NHE6 at excitatory presynaptic terminals suggests it may be a potential candidate and merits further investigation.

Recently, another member of the NHE family, the plasma membrane-type Na^+-selective NHE5 isoform that is enriched in brain tissue, has been found to shuttle between an intracellular vesicular pool and the cell surface of a subset of excitatory postsynaptic spines of rat hippocampal neurons in an activity-dependent manner (Diering et al., 2011). Interestingly, knockdown of NHE5 expression induced the enlargement as well as density of dendritic spines; alterations that were prevented by antagonists of NMDA receptors. While the precise mechanism underlying these effects is uncertain, it was proposed that insertion of NHE5 at the plasma membrane drives acidification of the synaptic cleft, which in turn negatively regulates NMDA receptor activity and spine morphogenesis. Whether NHE6 also modulates spine formation and synaptic function in a similar manner or plays a more fundamental role in intravesicular pH/cation homeostasis and vesicle trafficking remains to be explored.

In summary, this study provides the first evidence of NHE6 localization to excitatory synapses where it has the potential to contribute to learning and memory processes. NHE6 is present in excitatory axons, principal dendrites, and dendritic spines of mouse hippocampal neurons, but is also detected in protoplasmic astrocytes. Furthermore, NHE6 is developmentally regulated and undergoes activity-dependent modulation during LTP. Localization of this exchanger at excitatory synapses in hippocampal neurons suggests that deficiencies in its expression and/or catalytic activity as a result of genetic mutations could directly contribute to the cognitive dysfunction seen in affected individuals.

References

Blanpied TA, Scott DB, Ehlers MD (2002) Dynamics and regulation of clathrin coats at specialized endocytic zones of dendrites and spines. Neuron 36:435–449. CrossRef Medline

Bourne J, Harris KM (2007) Do thin spines learn to be mushroom spines that remember? Curr Opin Neurobiol 17:381–386. CrossRef Medline

Brett CL, Wei Y, Donowitz M, Rao R (2002) Human Na+/H+ exchanger isoform 6 is found in recycling endosomes of cells, not in mitochondria. Am J Physiol Cell Physiol 282:C1031–C1041. Medline

Brown TC, Tran IC, Backos DS, Esteban JA (2005) NMDA Receptor-dependent activation of the small GTPase Rab5 drives the removal of synaptic AMPA Receptors during hippocampal LTD. Neuron 45:81–94. CrossRef Medline

Brown TC, Correia SS, Petrok CN, Esteban JA (2007) Functional compartmentalization of endosomal trafficking for the synaptic delivery of AMPA receptors during long-term potentiation. J Neurosci 27:13311–13315. CrossRef Medline

Burry RW (2000) Specificity controls for immunocytochemical methods. J Histochem Cytochem 48:163–166. CrossRef Medline

Cameron PL, Südhof TC, Jahn R, De Camilli P (1991) Colocalization of synaptophysin with transferrin receptors: implications for synaptic vesicle biogenesis. J Cell Biol 115:151–164. CrossRef Medline

Chavez RA, Miller SG, Moore HP (1996) A biosynthetic regulated secretory pathway in constitutive secretory cells. J Cell Biol 133:1177–1191. CrossRef Medline

Cooney JR, Hurlburt JL, Selig DK, Harris KM, Fiala JC (2002) Endosomal compartments serve multiple hippocampal dendritic spines from a widespread rather than a local store of recycling membrane. J Neurosci 22:2215–2224. Medline

Coorssen JR, Schmitt H, Almers W (1996) Ca2+ triggers massive exocytosis in Chinese hamster ovary cells. EMBO J 15:3787–3791. Medline

Dailey ME, Smith SJ (1996) The dynamics of dendritic structure in developing hippocampal slices. J Neurosci 16:2983–2994. Medline

Davies J, Evans RH, Herrling PL, Jones AW, Olverman HJ, Pook P, Watkins JC (1986) CPP, a new potent and selective NMDA antagonist. depression of central neuron responses, affinity for [3H]d-AP5 binding sites on brain membranes and anticonvulsant activity. Brain Res 382:169–173.

Dean C, Dunning FM, Liu H, Bomba-Warczak E, Martens H, Bharat V, Ahmed S, Chapman ER (2012) Axonal and dendritic synaptotagmin isoforms revealed by a pHluorin-syt functional screen. Mol Biol Cell 23:1715–1727. CrossRef Medline

De Paola V, Arber S, Caroni P (2003) AMPA receptors regulate dynamic equilibrium of presynaptic terminals in mature hippocampal networks. Nat Neurosci 6:491–500. Medline

Diering GH, Mills F, Bamji SX, Numata M (2011) Regulation of dendritic spine growth through activity-dependent recruitment of the brain-enriched Na+/H+ exchanger NHE5. Mol Biol Cell 22:2246–2257. CrossRef Medline

Ehlers MD (2000) Reinsertion or degradation of AMPA receptors determined by activity-dependent endocytic sorting. Neuron 28:511–525. CrossRef Medline

Engert F, Bonhoeffer T (1999) Dendritic spine changes associated with hip-

pocampal long-term synaptic plasticity. Nature 399:66–70. CrossRef Medline

Fiala JC, Feinberg M, Popov V, Harris KM (1998) Synaptogenesis via dendritic filopodia in developing hippocampal area CA1. J Neurosci 18: 8900–8911. Medline

Fiala JC, Spacek J, Harris KM (2002) Dendritic spine pathology: cause or consequence of neurological disorders? Brain Res Rev 39:29–54. CrossRef Medline

Fortin DA, Davare MA, Srivastava T, Brady JD, Nygaard S, Derkach VA, Soderling TR (2010) Long-term potentiation-dependent spine enlargement requires synaptic Ca2+-permeable AMPA receptors recruited by CaM-kinase I. J Neurosci 30:11565–11575. CrossRef Medline

Gähwiler BH, Capogna M, Debanne D, McKinney RA, Thompson SM (1997) Organotypic slice cultures: a technique has come of age. Trends Neurosci 20:471–477. CrossRef Medline

Gähwiler BH, Thompson SM, McKinney RA, Debanne D, Robertson RT (1998) Organotypic slice cultures of neural tissue. In: Culturing nerve cells, Ed 2 (Banker G, Goslin K, eds). Cambridge, MA: MIT.

Garbern JY, Neumann M, Trojanowski JQ, Lee VM, Feldman G, Norris JW, Friez MJ, Schwartz CE, Stevenson R, Sima AA (2010) A mutation affecting the sodium/proton exchanger, SLC9A6, causes mental retardation with tau deposition. Brain 133:1391–1402. CrossRef Medline

Gerges NZ, Backos DS, Esteban JA (2004) Local control of AMPA receptor trafficking at the postsynaptic terminal by a small GTPase of the Rab family. J Biol Chem 279:43870–43878. CrossRef Medline

Gerges NZ, Backos DS, Rupasinghe CN, Spaller MR, Esteban JA (2006) Dual role of the exocyst in AMPA receptor targeting and insertion into the postsynaptic membrane. EMBO J 25:1623–1634. CrossRef Medline

Gilfillan GD, et al. (2008) SLC9A6 mutations cause X-linked mental retardation, microcephaly, epilepsy, and ataxia, a phenotype mimicking Angelman syndrome. Am J Hum Genet 82:1003–1010. CrossRef Medline

Goh GY, Huang H, Ullman J, Borre L, Hnasko TS, Trussell LO, Edwards RH (2011) Presynaptic regulation of quantal size: K+/H+ exchange stimulates vesicular glutamate transport. Nat Neurosci 14:1285–1292. CrossRef Medline

Harris KM, Jensen FE, Tsao B (1992) Three-dimensional structure of dendritic spines and synapses in rat hippocampus (CA1) at postnatal day 15 and adult ages: implications for the maturation of synaptic physiology and long-term potentiation. J Neurosci 12:2685–2705. Medline

Higgins D, Banker G (1998) Primary dissociated cell cultures. In: Culturing nerve cells, Ed 2 (Banker G, Goslin K, eds). Cambridge, MA: MIT.

Holtmaat AJ, Trachtenberg JT, Wilbrecht L, Shepherd GM, Zhang X, Knott GW, Svoboda K (2005) Transient and persistent dendritic spines in the neocortex in vivo. Neuron 45:279–291. CrossRef Medline

Jiang M, Chen G (2006) High Ca2+-phosphate transfection efficiency in low-density neuronal cultures. Nat Protoc 1:695–700. CrossRef

Johnson JW, Ascher P (1987) Glycine potentiates the NMDA response in cultured mouse brain neurons. Nature 325:529–531. CrossRef Medline

Kasai H, Fukuda M, Watanabe S, Hayashi-Takagi A, Noguchi J (2010) Structural dynamics of dendritic spines in memory and cognition. Trends Neurosci 33:121–129. CrossRef Medline

Kennedy MJ, Ehlers MD (2006) Organelles and trafficking machinery for postsynaptic plasticity. Annu Rev Neurosci 29:325–362. CrossRef Medline

Kennedy MJ, Ehlers MD (2011) Mechanisms and function of dendritic exocytosis. Neuron 69:856–875. CrossRef Medline

Kennedy MJ, Davison IG, Robinson CG, Ehlers MD (2010) Syntaxin-4 defines a domain for activity-dependent exocytosis in dendritic spines. Cell 141:524–535. CrossRef Medline

Kopec CD, Li B, Wei W, Boehm J, Malinow R (2006) Glutamate receptor exocytosis and spine enlargement during chemically induced long-term potentiation. J Neurosci 26:2000–2009. CrossRef Medline

Kopec CD, Real E, Kessels HW, Malinow R (2007) GluR1 links structural and functional plasticity at excitatory synapses. J Neurosci 27:13706–13718. CrossRef Medline

Lau CG, Takayasu Y, Rodenas-Ruano A, Paternain AV, Lerma J, Bennett MV, Zukin RS (2010) SNAP-25 is a target of protein kinase c phosphorylation critical to NMDA receptor trafficking. J Neurosci 30:242–254. CrossRef Medline

Lein E, wide atlas of gene expression in the adult mouse brain. Nature 445: 168–176. CrossRef Medline

Lin JW, Ju W, Foster K, Lee SH, Ahmadian G, Wyszynski M, Wang YT, Sheng M (2000) Distinct molecular mechanisms and divergent endocytotic pathways of AMPA receptor internalization. Nat Neurosci 3:1282–1290. CrossRef Medline

Lu J, Helton TD, Blanpied TA, Rácz B, Newpher TM, Weinberg RJ, Ehlers MD (2007) Postsynaptic positioning of endocytic zones and AMPA receptor cycling by physical coupling of dynamin-3 to homer. Neuron 55: 874–889. CrossRef Medline

Lu W, Man H, Ju W, Trimble WS, MacDonald JF, Wang YT (2001) Activation of synaptic NMDA receptors induces membrane insertion of new AMPA receptors and LTP in cultured hippocampal neurons. Neuron 29:243–254. CrossRef Medline

Lynch MA (2004) Long-term potentiation and memory. Physiol Rev 84:87–136. CrossRef Medline

Madrigal I, Fernández-Burriel M, Rodriguez-Revenga L, Cabrera JC, Mart í M, Mur A, Mil à M (2010) Xq26.2-q26.3 microduplication in two brothers with intellectual disabilities: clinical and molecular characterization. J Hum Genet 55:822–826. CrossRef

Malenka RC, Nicoll RA (1999) Long-term potentiation–a decade of progress? Science 285:1870–1874. CrossRef Medline

Matsuo N, Reijmers L, Mayford M (2008) Spine-type-specific recruitment of newly synthesized AMPA receptors with learning. Science 319:1104–1107. CrossRef Medline

McKinney RA (2010) Excitatory amino acid involvement in dendritic spine formation, maintenance and remodelling. J Physiol 588:107–116. CrossRef Medline

Morimoto T, Popov S, Buckley KM, Poo MM (1995) Calcium-dependent transmitter secretion from fibroblasts: Modulation by synaptotagmin I. Neuron 15:689–696. CrossRef Medline

Morrow EM, et al. (2008) Identifying autism loci and genes by tracing recent shared ancestry. Science 321:218–223. CrossRef Medline

Mundigl O, Matteoli M, Daniell L, Thomas-Reetz A, Metcalf A, Jahn R, De Camilli P (1993) Synaptic vesicle proteins and early endosomes in cultured hippocampal neurons: differential effects of Brefeldin A in axon and dendrites. J Cell Biol 122:1207–1221. CrossRef Medline

Nakamura N, Tanaka S, Teko Y, Mitsui K, Kanazawa H (2005) Four Na+/H+ exchanger isoforms are distributed to Golgi and post-Golgi compartments and are involved in organelle pH regulation. J Biol Chem 280:1561–1572. Medline

Numata M, Petrecca K, Lake N, Orlowski J (1998) Identification of a mitochondrial Na+/H+exchanger. J Biol Chem 273:6951–6959. CrossRef Medline

Ohgaki R, Fukura N, Matsushita M, Mitsui K, Kanazawa H (2008) Cell surface levels of organellar Na+/H+ exchanger isoform 6 are regulated by interaction with RACK1. J Biol Chem 283:4417–4429. Medline

Ohgaki R, Matsushita M, Kanazawa H, Ogihara S, Hoekstra D, van Ijzendoorn SC (2010) The Na+/H+ exchanger NHE6 in the endosomal recycling system is involved in the development of apical bile canalicular surface domains in HepG2 cells. Mol Biol Cell 21:1293–1304. CrossRef Medline

Park M, Penick EC, Edwards JG, Kauer JA, Ehlers MD (2004) Recycling endosomes supply AMPA receptors for LTP. Science 305:1972–1975. CrossRef Medline

Park M, Salgado JM, Ostroff L, Helton TD, Robinson CG, Harris KM, Ehlers MD (2006) Plasticity-induced growth of dendritic spines by exocytic trafficking from recycling endosomes. Neuron 52:817–830. CrossRef Medline

Penzes P, Cahill ME, Jones KA, VanLeeuwen JE, Woolfrey KM (2011) Dendritic spine pathology in neuropsychiatric disorders. Nat Neurosci 14: 285–293. CrossRef Medline

Petrini EM, Lu J, Cognet L, Lounis B, Ehlers MD, Choquet D (2009) Endocytic trafficking and recycling maintain a pool of mobile surface AMPA receptors required for synaptic potentiation. Neuron 63:92–105. CrossRef Medline

Prekeris R, Klumperman J, Chen YA, Scheller RH (1998) Syntaxin 13 mediates cycling of plasma membrane proteins via tubulovesicular recycling endosomes. J Cell Biol 143:957–971. CrossRef Medline

Rácz B, Blanpied TA, Ehlers MD, Weinberg RJ (2004) Lateral organization of endocytic machinery in dendritic spines. Nat Neurosci 7:917–918. CrossRef Medline

Rasband WS (1997–2008) ImageJ, U.S. National Institutes of Health, Bethesda, MD.

Richards DA, Mateos JM, Hugel S, de Paola V, Caroni P, Gähwiler BH,

McKinney RA (2005) Glutamate induces the rapid formation of spine head protrusions in hippocampal slice cultures. Proc Natl Acad Sci U S A 102:6166–6171. CrossRef Medline

Roche KW, Standley S, McCallum J, Dune Ly C, Ehlers MD, Wenthold RJ (2001) Molecular determinants of NMDA receptor internalization. Nat Neurosci 4:794–802. CrossRef Medline

Rotin D, Grinstein S (1989) Impaired cell volume regulation in Na(+)-H+ exchange-deficient mutants. Am J Physiol 257:C1158–C1165. Medline

Shahi K, Baudry M (1993) Glycine-induced changes in synaptic efficacy in hippocampal slices involve changes in AMPA receptors. Brain Res 627: 261–266. CrossRef Medline

Shepherd JD, Huganir RL (2007) The cell biology of synaptic plasticity: AMPA receptor trafficking. Annu Rev Cell Dev Biol 23:613–643. CrossRef Medline

Sorra KE, Harris KM (2000) Overview on the structure, composition, function, development, and plasticity of hippocampal dendritic spines. Hippocampus 10:501–511. CrossRef Medline

Spacek J, Harris KM (1997) Three-dimensional organization of smooth endoplasmic reticulum in hippocampal CA1 dendrites and dendritic spines of the immature and mature rat. J Neurosci 17:190–203. Medline

Strømme P, Dobrenis K, Sillitoe RV, Gulinello M, Ali NF, Davidson C, Micsenyi MC, Stephney G, Ellevog L, Klungland A, Walkley SU (2011) X-linked Angelman-like syndrome caused by Slc9a6 knockout in mice exhibits evidence of endosomal-lysosomal dysfunction. Brain 134:3369–3383. CrossRef Medline

Suh YH, Terashima A, Petralia RS, Wenthold RJ, Isaac JT, Roche KW, Roche PA (2010) A neuronal role for SNAP-23 in postsynaptic glutamate receptor trafficking. Nat Neurosci 13:338–343. CrossRef Medline

Tabb JS, Kish PE, Van Dyke R, Ueda T (1992) Glutamate transport into synaptic vesicles. Roles of membrane potential, pH gradient, and intravesicular pH. J Biol Chem 267:15412–15418. Medline

Takahashi Y, Hosoki K, Matsushita M, Funatsuka M, Saito K, Kanazawa H, Goto Y, Saitoh S (2011) A loss-of-function mutation in the SLC9A6 gene causes X-linked mental retardation resembling Angelman syndrome. Am J Med Genet B Neuropsychiatr Genet 156B:799–807. CrossRef

Tzschach A, Ullmann R, Ahmed A, Martin T, Weber G, Decker-Schwering O, Pauly F, Shamdeen MG, Reith W, Oehl-Jaschkowitz B (2011) Christianson syndrome in a patient with an interstitial Xq26.3 deletion. Am J Med Genet A 155A:2771–2774. CrossRef Medline

Wang Z, Edwards JG, Riley N, Provance DW Jr, Karcher R, Li XD, Davison IG, Ikebe M, Mercer JA, Kauer JA, Ehlers MD (2008) Myosin Vb mobilizes recycling endosomes and AMPA receptors for postsynaptic plasticity. Cell 135:535–548. CrossRef Medline

Weisz OA (2003) Organelle acidification and disease. Traffic 4:57–64. CrossRef Medline

Wilson JM, Colton TL (1997) Targeting of an intestinal apical endosomal protein to endosomes in nonpolarized cells. J Cell Biol 136:319–330. CrossRef Medline

Xinhan L, Matsushita M, Numaza M, Taguchi A, Mitsui K, Kanazawa H (2011) Na+/H+ exchanger isoform 6 (NHE6/SLC9A6) is involved in clathrin-dependent endocytosis of transferrin. Am J Physiol Cell Physiol 301:C1431–C1444. CrossRef Medline

Yoshimori T, Keller P, Roth MG, Simons K (1996) Different biosynthetic transport routes to the plasma membrane in BHK and CHO cells. J Cell Biol 133:247–256. CrossRef Medline

Yuste R, Bonhoeffer T (2001) Morphological changes in dendritic spines associated with long-term synaptic plasticity. Annu Rev Neurosci 24: 1071–1089. CrossRef Medline

Yuste R, Bonhoeffer T (2004) Genesis of dendritic spines: insights from ultrastructural and imaging studies. Nat Rev Neurosci 5:24–34. CrossRef Medline